

Responses to Reviewer(1)'s Comments:

We appreciate the reviewer's comments and suggestions, which were very helpful in improving the overall quality of our manuscript. Basically, all the comments and suggestions were reflected in our revision. Our responses are listed below to each comment.

Interactive comment on "Integration of GOCI and AHI Yonsei Aerosol Optical Depth Products During the 2016 KORUS-AQ and 2018 EMeRGe Campaigns" by Hyunkwang Lim et al.

This paper merges and analyzes aerosol optical depth (AOD) data from four data sets (two sensors – AHI and GOCI – each with two different algorithm versions) by two methods (simple mean and maximum likelihood) during two field campaigns in East Asia. Individual and merged data sets are evaluated against Sun photometer observations (more dense than usual due to the field campaigns); statistics of the individual product comparison are also used to inform the merging process for maximum likelihood. The paper is relevant to the journal and the special issue. The topic is important: we have a lot of satellite AOD data sets now and the question of merging comes up increasingly often. It is also nice to see the geostationary data here; this is a novel aspect and these new sensors offer temporal coverage unavailable from polar platforms (as the authors point out). So this is all good. The quality of language is ok: the authors have done a good job considering their native languages are not English, but some copy-editing will be required. This can probably be handled by the journal. As a result I have only made language comments when it relates to technical issues.

Some of the analysis is unclear, in particular, relating to the bias correction step (see later comments). I also found the organization of the paper hard to follow: a lot of different merging results were presented but the main message is not clear and I am not sure how well these results could be generalized to other time periods (outside of these field campaigns) or other data sets. Right now it is hard to tell if this is more a paper about these field campaigns, or these retrieval algorithms, or merging in general, because it's not focused/in depth enough. As a result I recommend major revisions to address these issues. My main recommendations relate to streamlining the analysis and discussion, and using more modern merge techniques. I would like to review the revised version. Specific comments in support of my recommendation are below:

1. Line 31: "affect radiative energy" should probably say "affect Earth's radiative energy balance" or "affect solar and thermal radiation" as the current wording feels a little odd.

- *Thank you for your comment. We revised this sentence.*

2. Lines 38-49: there are long citation lists here, with some repetition, and not really much discussion. I suggest consolidating this. We know there are many AOD retrieval algorithms, there's no value in listing a bunch of references unless they are discussed in more detail (as in the examples in the next paragraph). This is an issue elsewhere in the introduction as well, but especially here.

- *The inserted reference in the sentence was deleted.*

3. Line 50: DT is not one algorithm. It is two algorithms: one for land, one for water. They have the same name, but the assumptions (e.g. aerosol properties, surface reflectance) have nothing in common and even the channels used are different. This should be corrected.

- *Thank you for your comment. However, the DT-ocean and DT-land algorithms are often referred to as DT algorithms. Each algorithm's characteristics (land and ocean) are briefly mentioned in line 53-59.*

4. Lines 111-125: here the authors describe a number of approaches which have been used to merge AOD products. Given the sophistication of many of these methods, why are such simple methods (i.e. simple mean, and MLE – which is essentially an uncertainty-weighted mean) used in the present study? Why not use something more state-of-the-art? This paper seems a bit of a missed opportunity to study whether more advanced data fusion approaches as cited in these lines do any better than simple mean or MLE. The authors might consider trying to add a more advanced technique.

- *Previous studies mentioned in this paper include data fusion based on Kriging, reproduction of spectral AOD, and BME method. Most of them focus on gap filling and rebuild AOD in areas not observed by MISR, MODIS, and SeaWiFS, and so on (Wang et al., 2013; Tang et al., 2016). Here we focus on a study that attempts to improve the accuracy of AOD products at the retrieved pixels, thus shows the ensemble mean and MLE fusion, respectively, to compare these two, one very simple one and the other with more elaborated processes. Because the previous studies on AOD*

fusion improved the retrieved values mainly based on MLE or NDVI-based fusion studies (Wei et al., 2019, Levy et al., 2013), we tried to further improve them with rather simple approach to save computation time considering the nature of satellite product file size and user's near-real-time demand for data assimilation. Compared to the AERONET, the MLE method improved the scattered results of the satellite AOD, but did not correct the systematic bias, so additional bias correction was performed.

In addition, most of the fusion methods do not consider the uncertainties in each AOD product used, especially the uncertainty in the pixel scale. While some fusion algorithms do consider the uncertainty of source data, they rarely consider the systematic error of the product itself when calculating the uncertainty (Xu et al., 2015; Xie et al., 2018).

5. Section 2: I did not find a clear description of what wavelength(s) AOD is reported at in this analysis. From a few figure captions I think 550 nm, but this seems to be the only mention in the text. This should be stated clearly for each data set used, along with any method for spectral interpolation applied.

- Thank you for your comment. We added the wavelength information on Line 134, 150, 208 (revised manuscript).

6. Line 161: is 0.02 mg/m³ correct? This seems unrealistically low. I was surprised so looked through the Yamada paper cited and did not find this number supported. It looks (e.g. their Figure 2) that most of the time, for their limited domain, the climatological value is 0.1-1 mg/m³. However there is considerable variation. So using 0.02 seems wrong, and having no spatial/monthly variation also seems like it would introduce seasonal biases.

- Sorry for confusing. We removed reference.

0.02 represents the average climate value over clean ocean, and the sentence was revised.

In addition, 0.02mg/m³ used in the AHI ESR method was used only for CHL pixels that were not retrieved by the JAXA algorithm(Murakami. 2016), and according to Lim et al. (Remote Sensing, 2018), the maximum AOD error according to the CHL-a concentration of 50 mg/m³ in the YAER algorithm was 0.08.

7. Lines 234-244 and Table 1: This is where things get messy for me. I feel there are too many comparisons (7 merge tests, 4 un-merged data sets) and it gets difficult to remember which combinations of algorithm acronym belong to each data merge acronym without going back and forth to the table each time. Further, I am not sure that the split as presented enables the analysis authors want to do. It is complicated because we are splitting between not only different merge types, but also different numbers of sensors (as GOCI has a smaller disk), and also different observation regions (and we know aerosol and surface characteristics, as well as retrieval errors, are probably different in these regions). It is not comparing apples to apples. After reading the paper several times, I'm still not very sure what the message is and how general this recommendation might be. I wonder if it makes more sense to drop some of these experiments and focus only on the ones involving the GOCI disk in order to have a clearer picture for the analysis (consistent spatial domain, smaller number of comparisons, smaller region to map to make figures easier to read). Maybe doing this, and adding a more advanced merge method (see earlier comment), would give an analysis which is easier to follow and of broader interest. Having all the 11-panel figures which look mostly quite similar is hard to follow.

- Thank you for your comment. FM1 (MLE all) was selected as the representative fused AOD, and the domain area was reduced to GOCI's coverage. Other products were shown as differences from the FM1. Thanks to this update, the difference in fusion is well expressed.

8. Section 3.4: this section doesn't seem to actually explain how the bias correction was done. More detail is needed. Also, I don't see the evidence that retrieval errors do follow a Gaussian distribution: there is no Gaussian distribution comparison shown in Figure 1. This could be demonstrated better by e.g. a QQ plot. Further, it could be that there are multiple populations in here and it looks reasonably Gaussian on average, but not for subsets of the data.

- Thank you for your comment. We added more detail in the bias correction in section 3.4 and revised the Q-Q plot.

9. Line 264: Sayer (2013) does not show AOD follows a lognormal distribution. Perhaps the authors are thinking of Sayer and Knobelspiese (2019)? <https://acp.copernicus.org/articles/19/15023/2019/>

- Sorry for the confusion. We revised with the reference given by the reviewer's comment.

10. Sections 4, 5: these mostly just describe the figures and again, because there's a lot of maps and scatter plots which look very similar, it is hard to pick out the main message. This supports my idea to pick which experiments and parts of the data are most important and focus on those. In my view the figures should support the text; the text should clearly offer explanations and recommendations and not just describe the figures. I don't have many more specific comments on these for that reason.

- Thank you for your comment. We added and revised the figures, texts, and revised the conclusion.

11. Tables 2, 3: these are a bit of a sea of numbers. It is hard for the reader to parse them and extract the main message. If the variation between entries is important, perhaps these should be figures instead. Also, "NaN" does not belong in a table like this. If there were no data, leave it blank or put a "-". NaN is computer code.

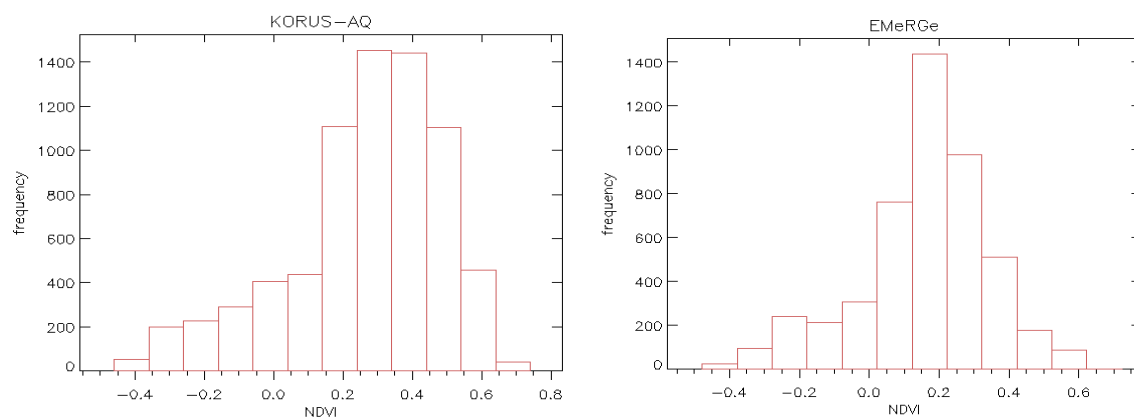
- Thank you for your comment. According to your comment, both Tables 2 and 3 were replaced with Figures 1 and 3. The period (2018.04-2019.03, but excluding the EMERGe campaign) was modified for statistical analysis to avoid data redundancy.

12. Figures 5, 7: I recommend the regression fits be removed here. As the authors note, AOD is close to lognormal. Also, the AOD error is dependent on AOD. Also, the fact that there are NDVI dependences of retrieval errors means that there are multiple populations of data with distinct characteristics here. All this means that the regression used is statistically inappropriate. It should be removed in order for the paper to be correct. I do not believe the regressions are vital to the discussion anyway.

- Thank you for your comment. We revised Figures 7 and 9.

13. Figure 9: can uncertainty bars be added here? It is hard to see whether these differences are real or within sampling error. Also, the x axis should be checked. While NDVI below zero is mathematically possible, it is not realistic except for water bodies or cloud-contaminated pixels. I am surprised that values seem to vary between -0.3 and +0.4 or so. Even deserts have an NDVI around 0.1-0.2, and vegetated areas often above 0.5. I wonder if there is perhaps a bug, a definition difference, or a serious spectral error in the surface reflectance model producing these values. This should be checked.

- For the collocation with AERONET, satellite AODs within 25km is averaged, which tends to decrease values partly, but it is confirmed that the maximum NDVI value is about 0.7. Also, negative NDVI appears because the ocean pixel (AERONET near coastal) is included. It may also look somewhat low because the average was taken as the representative value of the collocation points and plotted. The below figure shows the collocated NDVI values during each campaign period.



14. Figure 10: this has vertical bars but they are not explained. Is this standard deviation, standard error, or something else?

- Sorry for missing this. We added information of vertical bar, which was to show 1-sigma.

15. Conceptually, I also have an issue with using AERONET to train a bias correction and then evaluating the bias-corrected data against AERONET. Of course this will look better than the original products. I am not sure of the best way around this though. Again, streamlining the number of comparisons made in the paper will make it more readable and allow a better understanding of the advantages of the methods.

- The bias correction and RMSE were calculated using data for about one year from April 2018 to March 2019 (excluding the EMERGGe period) to avoid redundancy of all data. Therefore, we revised the results deviating from the cyclical logic that the reviewer told us because the error analysis was performed using the algorithm's characteristics for one year that does not overlap with a specific period.

Responses to Reviewer(2)'s Comments:

We appreciate the reviewer's comments and suggestions, which were very helpful in improving the overall quality of our manuscript. Basically, all the comments and suggestions were reflected in our revision. Our responses are listed below to each comment.

This article describes a study to compare different techniques for fusing aerosol optical depth products from two multi-spectral instruments viewing East Asia from geostationary orbit, GOCI and AHI, and evaluate the results during two field campaign periods. The topic is relevant given that these two instruments represent current state-of-the-art capabilities for diurnal aerosol observations from satellites. The hypothesis is that some type of ensemble mean will usually perform better than any individual member, and the paper compares 4 individual retrievals (2 each from GOCI and AHI), 4 different simple ensemble-mean combinations, and 3 different maximum-likelihood-estimate (MLE) combinations. In general, the hypothesis seems true, with the fused products generally overcoming different deficiencies in the individual products. However, the number of different permutations considered makes it difficult to focus on what attributes lead to the best improvements. The impact of bias correction should be clarified. Also, the current multi-panel figures make it difficult to see the differences. This work would make a valuable contribution to the literature if the clarity of the presentation can be improved. Specific suggestions are offered as follows.

SPECIFIC COMMENTS _____

The discussion of gap filling techniques starting at line 115 needs an introduction to provide context for the geostationary observations. While the need for gap filling in daily LEO observations is somewhat intuitive, it seems the simplest fusion of GEO products could produce a high yield without gap filling. Please clarify how the gap-filling applies to the current work.

- As reviewers commented, retrievals and applications using geostationary satellite observations cover many areas. Sorry for the lack of clarity in our originally submitted manuscript. Our aim was to provide optimized aerosol products from two different algorithm and two different instruments (GOCI and AHI). Therefore, this paper aims to produce the optimal fused AOD products where retrieved results are available, not to fill the gap where aerosol properties are not retrieved.

The organization of sections 2 and 3 was quite confusing to me; I had to re-read several times to understand what was being done. 2.1 is fine, simply describing the two AHI products. The first paragraph of 2.2 is fine, simply describing the two GOCI products. The second paragraph (beginning line 195) belongs in a separate section describing the different fusions, rather than in the GOCI algorithm section.

- Thank you for your comment. This part has been moved to the beginning of section 3.

Section 2.3 seems out of place; I suggest it be moved such that it is the last text before the Results section. Section 3 would greatly benefit from starting with a simple statement of the approach, e.g., we compare 4 different simple ensemble-mean combinations and 3 different MLE combinations. It is confusing to read about the MLE fusions in the Ensemble Mean section 3.2 (lines 242-244); I suggest you describe the FM entries of Table 1 in the next section about MLE method, instead of in this section about ensemble mean method. And at that point, note that the same members are included in F2 and FM2, F3 and FM3, F4 and FM1, as can be seen in Table 1. Further, I suggest you swap F1 and F4, so that the same members are included in F1 and FM1; this would make it easier for the reader to examine the differences in the figures. For example, adjacent panels (e) and (i) would be for the same members, similar to how adjacent panels (f,j) and (g,k) are for the same members, in Figs 2-3 and 5-8.

- Thanks for your suggestion to reorganize, which improves the manuscript story flow. In the next session, we revised our manuscript to mention FM1-3, and moved Sec 2.3 to the last paragraph before the results section. Also, we swapped F1 and F4, per reviewer's suggestion to improve readability.

Lines 256-261 (calculation of RMSE values) are confusing to me. If I understand correctly what you are doing, this could be explained much more clearly as follows. The locations of ground measurements are very sparse in comparison with the satellite coverage, so you choose to model RMSE as a function of NDVI. Then you bin all ground/satellite co-locations with respect to NDVI, AOD, and time, calculate the RMSE in each bin, and then apply this RMSE to every satellite pixel as a table lookup based on those 3 parameters.

- Thank you for your advice. We revised these sentences.

A similar comment applies to the description of bias correction technique (section 3.4, lines 267-272). It appears that bias correction is applied to the MLE fusions but not to the simple-mean fusions. It seems that bias-correcting the simple-mean fusions could easily be done and would provide a more direct comparison of the two techniques. And if you do this, you should be able to say something about the importance of bias correction in isolation.

- *The simple average fusion field is an ensemble averaging technique, which utilizes the characteristic of finding a better value when multiple signals are averaged. In the main texts, we would like to mention that the accuracy becomes better (the less scattered), as we have more ensemble members. Our purpose was to show how well they matched the MLE fusion products through bias correction and pixel-based error fusion. However, to demonstrate the comments pointed out by the reviewers, the result of performing the bias correction is attached below*

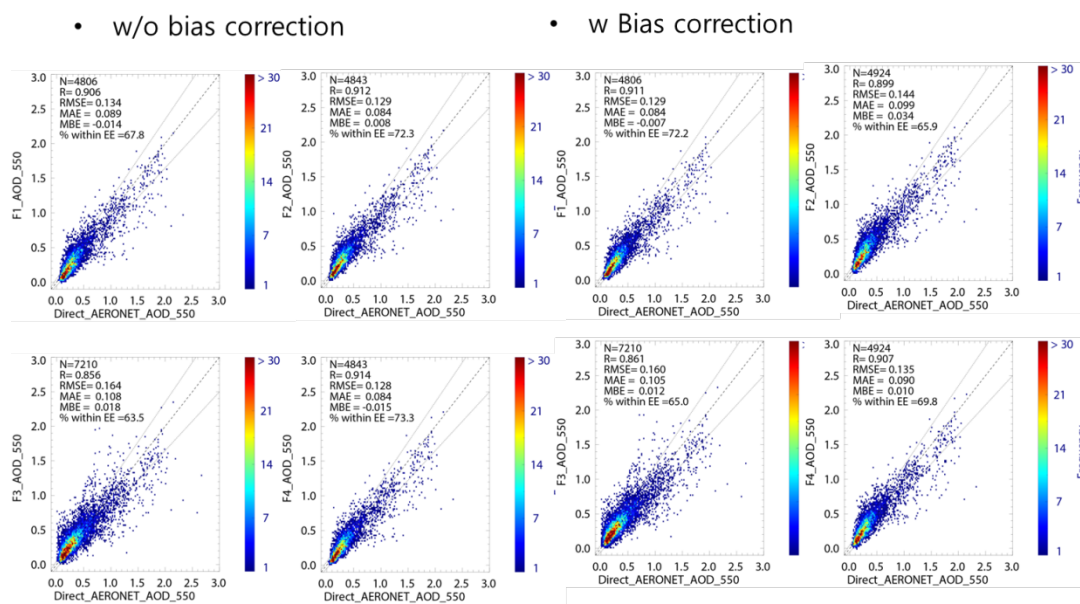


Figure 1. KORUS-AQ campaign

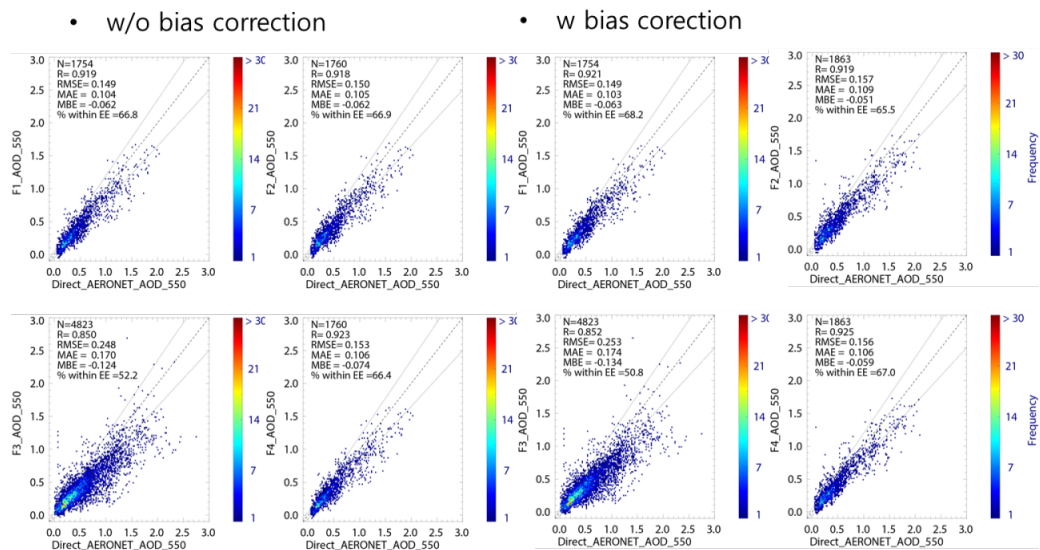


Figure 2. EMERGE campaign.

- Looking at the effect of bias correction, F1 using all outputs shows an improvement results. Meanwhile, F4, which uses an ensemble member similar to F1, decreases in KORUS-AQ and increases %EE in the EMERGE campaign. This may appear because the GV1's bias correction value is not accurate. Although mentioned in the text, the accurate correction may not be made using the RMSE and bias correction in this study for long-term analysis values. In general, if bias correction is performed and ensemble averaging is performed, MBE is improved in most cases, but the difference in EMERGE F3 product is the greatest.

The panels in figures 2, 3, 6, and 8 are so small that it is very difficult to see the differences in any features. Also, the large-domain view is only relevant for 4 cases (AER, AMR, F3, FM3). I suggest splitting each of these figures into 2 figures. The first would be for the large domain and would only have 4 panels, so the panels could all be twice as large. The second would be for the small (GOCI) domain and although it would have the same number of panels, there would be much less wasted white space since you would be zoomed into the GOCI region. Even with these changes, it may be difficult for the reader to actually see the differences among the cases. Consider selecting one product to show a representative AOD distribution (perhaps the one you consider to be the "best") and plot all other cases as the difference from this reference; this would allow you to clearly highlight where the differences arise.

- Thank you for your suggestion. We revised the Figure 4, 5 and paragraphs with one representative average AOD (FM1), while the remaining products were modified to show

differences, mean (XX) – mean (FM1), for the same area as the GOCI's.

It is very hard to see the differences in Figure 4. I suggest the figure could be greatly improved by plotting AERONET and DAOD (the difference from AERONET) for all the other products. The left vertical axis could be AOD and the right vertical axis could be DAOD. I don't think you would need a log scale.

- Thank you for your suggestion. DAOD was added as the reviewer suggested. However, if the figure is not shown in log-scale, the variation of the low AOD does not appear well, so the symbol thickness has been modified to be thin.

Line 335: The statement "the fusion products have a value of 0.131, lower than the minimum value of various satellite products (0.161)" is not true for all cases; Fused3 is .163, essentially the same as the .161 value quoted as the minimum of the individual products.

- Sorry for the confusion. We corrected sentence based on the re-calculated results, and added the phrase excluding F3, and FM3.

Paragraph beginning on line 349: This discussion highlights what I see as a problem with the current analysis. The AHI-only fusion results could also be analyzed within the small (GOCI) domain. Then there would be direct comparisons of all the ensembles in the small domain and separate comparisons of the large-domain results. I noted that Figure 11 does do this, which is the best aspect of Fig 11, and find it strange that this isn't done more consistently throughout the analysis.

- Thanks for the suggestion. As mentioned above, analysis domain was set as the GOCI domain in Figure 4 and 5. And, we added to section 5.3 and table 2. This section and table 2 were shown two AHI AODs validation score within GOCI's observation area.

First paragraph of section 5.2: AHI_ESR is in all the ensembles, so it is not surprising that the ensemble results move toward the AHI_ESR behavior. It explains the KORUS-AQ results; AHI_ESR has a positive bias, the other 3 have negative or no bias, so the combinations will produce small biases. Similar behavior is seen in EMeRGe; the results tend to collapse toward the original

AHI_ESR values. Discussion of Fig 11, in particular paragraph beginning on line 394: It is really impossible to see that "results after fusion show slightly better than respective satellite product accuracy in terms of SD, RMSE, and EE values" since so many points are clustered essentially on top of each other.

All that can be clearly seen is that GV1, GV2, and the "all" points are distinct from the cluster of everything else. It appears that the best discriminator between points in the cluster is the %EE. Two suggestions could improve this figure. First, in the legend, color the symbols by the %EE for each case, then at least it will be easy to see that it improves for the ensembles. Second, consider adding an inset that zooms in on the cluster of points. This may be irrelevant though (and Fig 11 redundant), if the result is that there are only minimal differences between the various cases.

- Thank you for your suggestion. The legend is also shown as %EE, and only all site validation is shown in the Taylor diagram as suggested by the reviewer. The validation of broader products collocated with GOCI is summarized in Table 2.

Line 410: This could also be because EMeRGe was in a period of brighter surface reflectance.

- Thank you for your comments. We added this point per the reviewer's comment.

Summary and Conclusion: I think it is important to point out that the ensemble-mean and MLE techniques produce very similar results, based on the numbers in Figures 5 and 7.

- Thank you for your comment. We added this point per the reviewer's comment.

Sentence on lines 433-435: This appears to be marginally true for EMeRGe (fig 7) but is not true for KORUS-AQ (fig 5), where ensemble-mean actually appears to be best.

- Thank you for your comment. We revised this sentence.

TECHNICAL CORRECTIONS _____

The citations on lines 48-49 duplicate citations earlier in the paragraph.

- We removed duplicate citations.

Line 195: unclear meaning; instead of the word "for", do you mean "depending on"?

- *We revised this word.*

Line 197: Not sure what is meant by "the NDVI shows a negative bias". Isn't NDVI an independent variable? Do you mean, when AOD is analyzed as a function of NDVI, a low bias exists for all values of NDVI?

- *Sorry for the confusion. We revised this sentence.*

Throughout, be consistent between the convention used in the text, tables, and figures. The text mostly uses the "short" labels e.g. as defined in lines 231-232, while the figures use a "long" convention that is much easier for the reader to keep straight (e.g., AHI_MRM instead of AMR). As a reader, I preferred the longer conventions because of this ease of keeping things straight.

- *Thank you for your comments. We revised that the abbreviations of the text and pictures have been unified.*

Line 240: define what is meant by "wide area". It becomes clear when looking at the figures, however at this point in the paper it would be helpful to define it.

- *Thank you for your suggestion. We added domain information.*

Line 266: Typo, AESR should be AES

- *Thank you for your comment. We removed this sentence.*

Line 382: Start a new paragraph for the discussion of Figure 11.

- *Thank you for your suggestion. We revised.*

Throughout the manuscript, be consistent with terminology. Fusion is the generic term. Two fusion techniques are used, ensemble mean and MLE. E.g., the legend in Fig 11 should indicate ensemble-mean rather than fusion.

- *Thank you for your comment. We revised the all of the legends.*

Line 429-430: It seems the biases are not "due to" NDVI etc., but instead are represented as functions of NDVI, time of day, and AOD.

- *Thank you for your comments. We revised this sentence.*

Tables 1 and 3: The NDVI labels are identical for the 2nd and 3rd groupings. It seems one or both are typographical errors.

- *Sorry for the confusion. We replaced the tables with figures.*

서식 지정함: 글꼴: 17 pt

Integration of GOCI and AHI Yonsei Aerosol Optical Depth Products During the 2016 KORUS-AQ and 2018 EMeRGe Campaigns

5 Hyunkwang Lim¹, Sujung Go^{1,2}, Jhoon Kim¹, Myungje Choi^{2,3}, Seoyoung Lee¹, Chang-Keun Song⁴, Yasuko Kasai⁵

¹Department of Atmospheric Sciences, Yonsei University, Seoul 03722, Republic of Korea

²Joint Center for Earth Systems Technology, University of Maryland Baltimore County, Baltimore, MD, USA

³Jet Propulsion Laboratory, California Institute of Technology, Pasadena, CA, USA

10 ⁴School of Urban and Environmental Engineering, Ulsan National Institute of Science and Technology, Ulsan 44919, Republic of Korea

⁵National Institute of Information and Communications Technology, Tokyo 184-8759, Japan

Correspondence to: Jhoon Kim (jkim2@yonsei.ac.kr)

15 **Abstract.** The Yonsei Aerosol Retrieval (YAER) algorithm for the Geostationary Ocean Color Imager (GOCI) retrieves aerosol optical properties only over dark surfaces, so it is important to mask pixels with bright surfaces. The Advanced Himawari Imager (AHI) is equipped with three shortwave-infrared and nine infrared channels, which is advantageous for bright-pixel masking. In addition, multiple visible and near-infrared channels provide a great advantage in aerosol property retrieval from the AHI and
20 GOCI. By applying the YAER algorithm to 10 minute AHI or 1 hour GOCI data at $6 \text{ km} \times 6 \text{ km}$ resolution, diurnal variations and aerosol transport can be observed, which has not previously been possible from low-earth-orbit satellites. This study attempted to estimate the optimal aerosol optical depth (AOD) for East Asia by data fusion, taking into account satellite retrieval uncertainty. The data fusion involved two steps: (1) analysis of error characteristics of each retrieved result with respect to the
25 ground-based Aerosol Robotic Network (AERONET), and bias correction based on normalized difference vegetation indexes; and (2) compilation of the fused product using ensemble-mean and maximum-likelihood estimation methods. Fused results show a better statistics in terms of fraction within the expected error, correlation coefficient, root-mean-square error, median bias error than the retrieved result for each product.

삭제함: s

삭제함: estimation

30 1. Introduction

Aerosols are generated by human activities and natural processes on local to global scales, and have a lifetime of several to tens of days. Aerosols affect Earth's radiative energy balance by scattering and absorption (e.g. Cho et al., 2003). High aerosol loadings are persistent in Northeast Asia, including diverse aerosol types from various sources. Interactions among aerosols, clouds, and radiation in the

서식 지정함: 글꼴: 12 pt

서식 있음: 들여쓰기: 첫 줄: 1 글자

atmosphere cause significant uncertainties in climate-model calculations (IPCC, 2013). Datasets produced by satellites have been widely used to reduce such uncertainties (Saide et al., 2014; Pang et al., 2018), but the systems must be accurately calibrated, verified, and consistent. Satellite data have been used extensively to retrieve aerosol optical properties (AOPs) over broad areas, with several algorithms having been developed. Satellites in low earth orbit (LEO), including Sun-synchronous orbit (SSO), cover the entire Earth over one to several days, depending on instrument and orbit characteristics. Most aerosol retrieval algorithms have been developed for LEO satellites (Kim et al., 2007; Lyapustin et al., 2011a, b; Lee et al., 2012; Fukuda et al., 2013; Hsu et al., 2013; Levy et al., 2013; Garay et al., 2017, 2020). LEO instruments currently onboard satellites include the Moderate Resolution Imaging Spectrometer (MODIS), Visible Infrared Imaging Radiometer Suite (VIIRS), Multi-angle Imaging SpectroRadiometer (MISR), and Cloud and Aerosol Imager (CAI) (Remer et al., 2005; Lyapustin et al., 2011a, b, 2018; Fukuda et al., 2013; Hsu et al., 2013; Levy et al., 2013; Garay et al., 2017, 2020; Lee et al., 2017).

Representative algorithms developed for MODIS data include the Dark-Target (DT; Remer et al., 2005; Levy et al., 2013), Deep Blue (DB; Hsu et al., 2013; Sayer et al., 2014), and Multi-Angle Implementation of Atmospheric Correction (MAIAC; Lyapustin et al., 2011a, b) systems, which are also applied for the succeeding VIIRS (Sayer et al., 2018). In the DT algorithm, the 2.1 μm channel is used to estimate land-surface reflectance in the visible (VIS) region using empirical equations based on the normalized difference vegetation index (NDVI). The DT algorithm has improved surface-reflectance modelling through consideration of the fractional area of urbanization (Gupta et al., 2016). Ocean-surface reflectance is estimated using the Cox and Munk method (Cox and Munk, 1954), and AOPs over land and ocean are provided at spatial resolutions of 10 km \times 10 km and 3 km \times 3 km (Remer et al., 2013), respectively. The DB algorithm has an advantage over the DT algorithm in allowing aerosol data retrieval over bright surfaces. By using a shorter-wavelength channel, accuracy is improved over bright surfaces such as urban and desert areas, where surface reflectance was previously estimated by the minimum reflectance method (MRM; Herman and Celarier 1997; Koelmeijer et al., 2003; Hsu et al., 2004). Furthermore, with the improvement to Collection 6.1, land-surface reflectance can be estimated similarly to the DT method, over densely vegetated regions (Sayer et al., 2019). In the case of VIIRS DB, aerosol retrieval over the ocean is also applied by the Satellite Ocean Aerosol Retrieval (SOAR) algorithm (Sayer et al., 2018). In the MODIS MAIAC system, surface reflectance is estimated by considering various images based on time-series analysis, with multi-angle observations, based on up to 16 day data, and by applying the bidirectional reflectance distribution function (BRDF). Ocean-surface reflectance is determined using a Cox and Munk BRDF model similar to DT and VIIRS DB (Lyapustin et al., 2011a, b, 2018). The MISR observes Earth at nine different angles, providing a high degree of freedom in signals; consequently, retrievals yield estimates of aerosol type and shape. As with the MAIAC, multiple observations are used, with the estimation of land-surface reflectance involving bidirectional reflectance factors (BRF). Zhang et al. (2016) developed an aerosol retrieval algorithm that allows aerosol data retrieval over bright land surfaces using surface-reflectance ratios from the VIIRS.

Aerosol retrieval algorithms for geosynchronous Earth orbit (GEO) satellites have been developed, including the Geostationary Operational Environmental Satellite (GOES) series in the USA (Knapp et al., 2005), Meteosat series in Europe (Bernard et al., 2011), Himawari series in Japan (Yoon et al., 2007;

삭제함: (Knapp et al., 2005; Remer et al., 2005; Kim et al., 2008; Lyapustin et al., 2011a, b; Lee et al., 2012; Fukuda et al., 2013; Hsu et al., 2013; Levy et al., 2013; Kim et al., 2014, 2016; Choi et al., 2016, 2018; Garay et al., 2017, 2020; Kikuchi et al., 2018; Li, et al., 2018). Sun-synchronous orbit (SSO) satellites pass over the same

삭제함: Sun-synchronous orbit (SSO) satellites pass over the same area each day at approximately the same local time. ...

삭제함: 1

서식 지정함: 글꼴: (영어) Times New Roman

Kim et al., 2008; Lim et al., 2018; Kikuchi et al., 2018; Yoshida et al., 2018; Gupta et al., 2019), and the Geostationary Korea Multi-Purpose Satellite (GEO-KOMPSAT, GK) series in South Korea (Kim et al., 2014, 2016; Choi et al., 2016, 2018; Kim et al., 2020). However, previously launched geostationary meteorological satellites had only a single, broadband VIS channel, with which it is difficult to retrieve AOPs other than aerosol optical depth (AOD) (Wang et al., 2003; Knapp et al., 2005; Kim et al., 2008, 2014, 2016; Bernard et al., 2011). However, the Geostationary Ocean Color Imager (GOCI) onboard the GK-1 satellite, also known as the Communication, Ocean, and Meteorological Satellite (COMS), has six VIS and two near-infrared (NIR) channels, which is advantageous for retrieving AOPs (Lee et al., 2010; Choi et al., 2016, 2018; Kim et al., 2017). Next-generation meteorological GEO satellite instruments, including the Advanced Himawari Imager (AHI), Advanced Baseline Imager (ABI), and Advanced Meteorological Imager (AMI), have three to four VIS and NIR channels, which enable aerosol property retrieval with high accuracy (Lim et al., 2016, 2018; Kikuchi et al., 2018; Yoshida et al., 2018; Gupta et al., 2019). Kikuchi et al. (2018) and Yoshida et al. (2018) performed aerosol retrievals using the MRM and corrected reflectance using empirical equations. Gupta et al. (2019) extended the MODIS DT algorithm to GEO satellites and estimated visible surface reflectance using SWIR reflectance. Lim et al. (2018) retrieved the AOPs using both MRM and estimated surface reflectance from short-wave IR (SWIR) data (estimated surface reflectance, ESR), and presented the two merged products: an L2-AOD merged product, and a reprocessed AOD produced by merging MRM and ESR surface reflectances.

Algorithms developed to date for LEO and GEO satellites have both advantages and disadvantages, depending on algorithm characteristics. Therefore, the MODIS team provides combined DT and DB AOD products (Levy et al., 2013; Sayer et al., 2014). In addition, several studies of the fusion of L2 products have been conducted (Levy et al., 2013; Sayer et al., 2014; Wei et al., 2019), with Bilal et al. (2017) obtaining reliable results from merged DT and DB products, as indicated by the NDVI in East Asia, and also robust products by simply averaging DT and DB without consideration of the NDVI. AOP data fusion in East Asia may also be achieved using aerosol products of AMI, GOCI-2, and the geostationary environment monitoring spectrometer (GEMS) onboard the GK-2A and 2B satellites launched by South Korea in 2018 and 2020, respectively, with accuracy over bright surfaces being improved by the GEMS aerosol product. It is also possible to obtain accurate AOPs, such as single-scattering albedo, aerosol loading height, and fine-mode fraction, which have been difficult to obtain by fusion of L2 data and/or surface reflectance data. If the trace-gas dataset retrieved from GEMS is used, it is possible to improve the aerosol type, with the retrieval of high-quality AOD data (Go et al., 2020).

Several studies have considered AOD data fusion, for which methods can be broadly classified into two types. First, the fusion of more than one AOD product may involve optimal interpolation (Xue et al., 2012), linear or second-order polynomial functions (Mélin et al., 2007), arithmetic or weighted means (Gupta et al., 2008), or maximum-likelihood estimates (MLE) (Nirala, 2008; Xu et al., 2015; Xie et al., 2018). Second, in the absence of satellite-derived AOD products for the day of fusion, the geostatistical fusion method, universal kriging method (Chatterjee et al., 2010; Li et al., 2014), geostatistical inverse modelling (Wang et al., 2013), or spatial statistical data fusion (Nguyen et al., 2012) may be applied. These have the advantage that AOD can be estimated by integrating the spatial autocorrelation of AOD data even for pixels missing from the AOD products, although there is a disadvantage in not considering temporal correlations. The Bayesian maximum entropy (BME) method, taking into account temporal

130 autocorrelation, has also been developed (Tang et al., 2016). BME methodology can estimate gap-filling
 pixels that are difficult to retrieve due to clouds, but with somewhat reduced accuracy. Gap filled AOD
 using the BME method, and satellite-derived AOD discontinuity arises from insufficient temporal
 sampling being available with the use of LEO satellites, resulting in a low fusion synergy. **Previous**
studies mentioned above include data fusion based on Kriging, reproduction of spectral AOD, and BME
method. Most of them focus on gap filling and rebuild AOD in areas not observed by MISR, MODIS,
and SeaWiFS, and so on (Wang et al., 2013; Tang et al., 2016). However in this study, we focused on
optimized AOD products with improved accuracy at the retrieved pixels by ensemble mean and MLE
fusion. We compared these two products, one very simple one and the other with more elaborated
processes. As previous AOD fusion studies improved the retrieved results mainly based on MLE or
NDVI-based fusion studies (Bilal et al., 2017; Levy et al., 2013; Wei et al., 2019; Go et al., 2020), we
tried to further improve them with efficient approach to save computation time considering the nature of
satellite data file size and user's near-real-time demand for data assimilation.

In this study, the GEO satellite dataset was used to resolve the temporal sampling issue for data fusion,
 while maintaining the spatio-temporal resolution retrieved from GEO satellites. We also attempted to
 estimate fused AOD products at 550nm with higher accuracy in East Asia. The ensemble-mean and
 MLE methods were applied. Section 2 describes the two algorithms used in this study for AHI and
 GOCI. Section 3 mentions methods of fusion and systematic bias correction, and section 4 performs
 validation of the fused products with the Aerosol Robotic Network (AERONET) instruments during
 two field campaigns: the Korea–United States Air Quality Study (KORUS-AQ) and the Effect of
 Megacities on the Transport and Transformation of Pollutants on Regional and Global Scales Study
 (EMeRGe).

2. Descriptions of AHI, GOCI, the YAER algorithm, and the two field campaigns

2.1 AHI aerosol algorithm

The Himawari-8 and -9 satellites were launched by the Japanese Meteorological Agency (JMA) on 7
 October 2014 and 2 November 2016, respectively. The AHI onboard these satellites has 16 channels
 covering wavelengths of 0.47–13.3 μm and performs full-disk and Japan-area observations every 10 and
 2.5 min, respectively, from GEO at 140.7° E longitude (Bessho et al., 2016). Visible and NIR
 observations are also performed at high spatial resolutions of 0.5–1.0 km, with SWIR to IR at 2 km,
 which have advantages in aerosol property retrieval and cloud masking.

Lim et al. (2018) developed the AHI Yonsei aerosol retrieval (YAER) algorithm and provided two
 retrieval results with 6 km × 6 km resolution at 550 nm based on MRM and ESR using SWIR data.
 Aerosol property retrieval using VIS channels requires accurate surface reflectance, for which MRM
 and ESR are useful, with the main difference between the two lying in the surface-reflectance
 estimation method.

The MRM applies the minimum-reflectance technique over both land and ocean (Lim et al., 2018),
 with surface reflectance being estimated by finding the minimum reflectance in each pixel over the past
 30 day window, giving the Lambertian equivalent reflectance (LER; Knapp et al., 2002; Wang et al.,

- 삭제함: So
- 삭제함: this study that attempts
- 삭제함: to
- 삭제함: AOD
- 삭제함: , thus showed
- 삭제함: the
- 삭제함: , respectively
- 삭제함: , to
- 삭제함: compare t
- 삭제함: Because
- 삭제함: the
- 삭제함: studies on
- 삭제함: pixels
- 삭제함: rather a simple
- 삭제함: product
- 서식 지정함: 글꼴: (한글) 바탕, (한글) 한국어
- 삭제함: and Sun-Sky Radiometer Observation Network (SONET)
- 서식 지정함: 글꼴: 12 pt

2003; Kim et al., 2008; Choi et al., 2016, 2018; Kim et al., 2016; Lim et al., 2018). This method takes the bidirectional characteristics of surface reflectance into consideration by obtaining surface reflectance at each observation time over the 30-day search window. However, the method assumes that during the search window there is more than one clear day and that surface reflectance does not change; otherwise, it is affected by clouds and/or the background aerosol optical depth (BAOD; Kim et al., 2014; Kim et al., 2021).

According to the ESR method, land-surface reflectance in the Vis region is constructed from the Top of Atmosphere (TOA) reflectance at 1.6 μm wavelength, based on the NDVI for SWIR and the fraction of urbanization and cropland (Levy et al 2013; Gupta et al., 2016; Zhong et al., 2016; Lim et al., 2018). Ocean-surface reflectance is estimated from the Cox and Munk BRDF model (Hsu et al., 2004; Lee et al., 2012; Jackson et al., 2013; Choi et al., 2016, 2018; Lim et al., 2018; Sayer et al., 2018).

Chlorophyll-a concentrations are considered in addition to data from Japan Aerospace Exploration Agency (JAXA) (Murakami et al., 2016) and interpolated for the 10-min AH1 intervals. For unretreived pixels, the less contaminated chlorophyll-a concentration value of 0.02 mg m^{-3} is used. Details of the methodology can be found in Lim et al. (2018).

The MRM gives better accuracy over brighter surfaces such as urban areas, while the ESR method gives better accuracy over areas of dense vegetation (Lim et al., 2018). However, there is a critical surface reflectance at which aerosol signals disappear, depending on the single-scattering albedo (Kim et al., 2016). Over the ocean, both the MRM and ESR methods give high accuracy, but ESR results are robust with the Cox and Munk model.

The MRM requires more computational time than the ESR method to estimate surface reflectance, as it requires data for the past 30 days, and LER needs to be calculated using a radiative transfer model. The ESR method estimates surface reflectance from the observed TOA reflectance at 1.6 μm wavelength using empirical equations including the NDVI. The advantage of MRM is that stable surface reflectance values can be obtained regardless of surface type. However, due to the influence of BAOD, surface reflectance tends to be overestimated, with satellite-derived AOD data thus being underestimated (Kim et al., 2014). On the other hand, the ESR method uses TOA reflectance at 1.6 μm wavelength to detect surface signals, which is less sensitive to fine particles and BAOD. However, when aerosols such as yellow dust with coarse particles are transported from the Taklamakan and Gobi deserts, the BAOD effect also applies to the ESR method. The ESR method is also more likely to be affected by snow surfaces than the MRM, as snow reduces reflectivity around the 1.6 μm wavelength (Negi and Kokhanovsky, 2011). The ESR method also has the disadvantage of giving noisy results over bright surfaces such as desert. However, its fast surface-reflectance estimation enables near-real-time retrieval based on the AH1 YAER algorithm.

2.2 GOCI aerosol algorithm

GOCI is an ocean color imager launched onboard COMS in 2010 and observes the East Asia region at an hourly interval with 500 $\text{m} \times 500 \text{m}$ resolution (Choi et al., 2012). It has eight bands in the VIS and NIR regions, which is advantageous for aerosol retrieval. Two versions of GOCI Yonsei aerosol algorithms have been developed, referred to as V1 and V2 (Lee et al., 2010; Choi et al., 2016, 2018). In the case of V1, surface reflectance is estimated by the MRM using LER for the past 30 days over land,

삭제함: C

서식 지정함: 위 첨자

삭제함: For unretreived pixels, the East Asian climatological value of 0.02 mg m^{-3} is used (Yamada et al., 2004). ...

서식 지정함: 글꼴: 12 pt

and the Cox and Munk BRDF model over oceans. In V2, ocean-surface reflectance is estimated by the same method, but land-surface reflectance is improved by using an accumulated long-term database. To minimize the impact of BAOD (the weakness of the MRM), a monthly surface-reflectance database was constructed using all of the LERs over the past five years, but it cannot reflect unexpected changes in surface conditions. However, a well-established climatological database allows aerosol property retrieval in near-real-time with reasonable accuracy.

3. Data fusion methods

Satellite-derived AODs have different error characteristics depending on NDVI, scattering angle, and so on (Choi et al., 2016, 2018; Lim et al., 2018). Over oceans, ESR AODs are more accurate than MRM AODs. However, the accuracy of GOCI, according to NDVI, has a negative bias for V1 and mostly a positive bias for V2 (Choi et al., 2018). In this study, we developed optimal AOD products at 550nm in East Asia by fusing four individual retrievals, i.e. two AHI aerosol products from the MRM and ESR methods, and two GOCI products from V1 and V2.

3.1 Spatio-temporal matching

The AHI and GOCI have different spatial pixel locations and temporal resolutions, so it is necessary to match their spatio-temporal resolutions before data fusion. GOCI and AHI AODs have the same spatial resolution of $6 \text{ km} \times 6 \text{ km}$, but the two satellites are located at 128.2° E and 140.7° E , respectively, at the equator. Spatial pixel matching is therefore required. However, satellite-derived AOD represents total-column extinction, so AOD retrieved by the two sensors is not significantly affected by satellite position. To merge the different satellite spatial pixel coverages, the GOCI pixel was re-gridded to match AHI pixels for full-disk observation, with up to 4 GOCI AOD pixels being used with average values considered representative of pixel values. If more than half of the AHI AOD pixels did not exist out of the maximum 6 AHI data per hour, it is regarded as cloud contaminated pixels and an additional cloud removal process is performed. This process applies to both the MRM and ESR method, to remove the AHI's additional cloud-contaminated pixels in products of both GOCI V1 and V2, which have a disadvantage in cloud masking due to their lack of IR channels. When three or more pixels were available for generating AHI data at 1 hour intervals, hourly AOD values were estimated as the medians of pixel values.

3.2 Ensemble mean method

Here, AMR represents AHI MRM AOD, AES represents AHI ESR AOD, GV1 represents GOCI V1 AOD, and GV2 represents GOCI V2 AOD. We performed data fusion using AMR, AES, GV1, and GV2 data within 1 hour intervals for which additional-cloud masking was performed. The ensemble mean is the mean of the ensemble member over a specific time. The ensemble members are AMR, AES, GV1, and GV2 based on two satellite instruments and two different surface-estimation methodologies. Table 1 provides the satellite-derived AOD used for ensemble-mean and MLE fusion.

삭제함: Satellite-derived AODs have different error characteristics for NDVI, scattering angle, and so on (Choi et al., 2016, 2018; Lim et al., 2018). Over oceans, ESR AODs are more accurate than MRM values. However, in GOCI, the NDVI shows a negative bias in V1 and positive bias in V2. In this study, we developed optimal AOPs in East Asia by fusing two AHI aerosol products from the MRM and ESR methods, and GOCI products from V1 and V2.⁴²

[1] 아래로 이동함: 2.3 Evaluation of aerosol products during two field campaigns⁴³
The performance of fused products was analyzed in two field campaigns: the KORUS-AQ of 1 May 2016 to 12 Jun 2016 (<https://www-air.larc.nasa.gov/missions/korus-aq/>), and EMERGE of 12 Mar 2018 to 8 Apr 2018 (<https://www.halo.dlr.de/science/missions/emerge/emerge.html>). KORUS-AQ was an international multi-organization mission to observe air quality across the Korean Peninsula and surrounding waters, led by the US National Aeronautics and Space Administration (NASA) and the Korean National Institute of Environmental Research (NIER). EMERGE aimed to investigate experimentally the patterns of atmospheric transport and transformation of pollution plumes originating from Eurasia, tropical and subtropical Asian megacities, and other major population centers. GEO satellite data played an important role in these campaigns; e.g., data assimilation for chemical transport models and tracking aerosol plumes (Saide et al., 2014; Pang et al., 2018; Saide et al., 2020). Here, we applied satellite-derived GOCI and AHI AODs, with a spatial resolution of $6 \text{ km} \times 6 \text{ km}$, and temporal resolutions of 1 hour and 10 minutes, respectively.⁴⁴

서식 지정함: 글꼴: 12 pt

서식 있음: 들여쓰기: 첫 줄: 1 글자

서식 지정함: 글꼴: 12 pt

서식 지정함: 글꼴: (영어) + 제목(Times New Roman)

삭제함: E

서식 지정함: 글꼴: 12 pt

Fusion was performed only when a pixel of an ensemble member was used for all fusions. Fusion 1 (F1) included the two AHI products of AMR and AES, and two GOCI products of GV1 and GV2. Fusion 2 (F2) involved the calculation of the YAER algorithm by the fusion of AES and GV2, both of which have the advantage of producing data in near-real-time. Fusion 3 (F3) merged AMR and AES to estimate AOD over a wide area, and Fusion 4 (F4) involved a comparison with F1 to determine how accuracy varied with decreasing number of ensemble members.

3.3 MLE method

Also, Table 1 shows the FM1 is the result of MLE fusion involving all satellite-derived AOD, and FM2 involves AER and GV2 for near-real-time operation. FM3 includes AMR and AES, enabling wide-area (70°-150 °E, 0°-50°N) observation.

The MLE method provides a means of weighting and averaging based on errors evaluated with AERONET ground-based measurements (Nirala, 2008; Xu et al., 2015; Xie et al., 2018).

This method employs the following equations:

$$\tau_i^{MLE} = \frac{\sum_{k=1}^N R_{i,k}^{-2} \tau_{i,k}}{\sum_{k=1}^N R_{i,k}^{-2}} \quad (1)$$

$$R_{i,k} = \sqrt{\frac{\sum_{i=1}^M (s_{i,k} - g_i)^2}{M}} \quad (2)$$

where τ_i^{MLE} represents the fused AOD; $\tau_{i,k}$ represents the mean AOD at grid point i from the satellite-derived AOD product k , where k is the index for different satellite-derived AOD products for fusion; $R_{i,k}$ represents the root-mean-square error (RMSE) at grid point i for the satellite-derived AOD product k ; N is the number of all AOD data; g_i represents the mean of ground-based AOD at grid point i from the AERONET (collocated temporal mean); $s_{i,k}$ represents the mean of satellite derived AOD products (k) at grid points of the AERONET (collocated spatial mean); and M is the number of pairs of $s_{i,k}$ and g_i .

Satellite observation can cover wide areas, but the ground observation instrument cannot cover all satellite observed areas. Therefore, a RMSE model was constructed for AOD, time, and NDVI through comparative validation with AERONET observation as shown in Figure 1. For MLE over wide areas without ground measurements, the calculated RMSE from AOD, time, and NDVI bins was applied for every satellite pixel. We excluded points that AOD differences with respect to AERONET data (dAOD) were > 2 standard deviations (SD) to remove outliers and to consider only the more stable RMSE values.

삭제함: ,
 삭제함: ,
 삭제함:

삭제함: increasing
 [2] 아래로 이동함: FM1 is the result of MLE fusion involving all satellite-derived AOD, and FM2 involves AER and GV2 for near-real-time operation. FM3 includes AMR and AES, enabling wide-area observation. ←

서식 지정함: 글꼴: 12 pt
 삭제함: n
 [2] 이동함(삽입)
 삭제함: was

서식 있음: 줄 간격: 1줄

삭제함: /S
 삭제함: ONET
 삭제함: /SONET
 삭제함: models
 삭제함: RMSE
 삭제함: were calculated
 삭제함: nd were
 삭제함: on those parameters
 삭제함: RMSE
 삭제함: by

삭제함: The RMSE used here was calculated by comparing average AERONET/SONET AODs over ±30 minutes intervals with respect to the satellite observation time, and AODs within 25 km of the AERONET/SONET site. For MLE over wide areas without ground measurements, the RMSE was estimated by grouping AODs based on NDVI bins; their values for the KORUS-AQ period are summarized in Table 2. We excluded points that

3.4 Bias correction

AOD follows a log-normal distribution (Sayer and Knobelspiesse, 2019), but dAOD for each satellite product follow a Gaussian distribution (Sayer et al., 2013). The quantile-quantile (Q-Q) plot is a graphical statistical technique that compares two probability distributions with each other. The x-axis represents the quantile value of the directly calculated sample, and the y-axis represents the Z-score. Here, the Z-score is a dimensionless value that makes a statistically Gaussian distribution and shows where each sample is located on the standard deviation. That is, when Z-score is 1 and 2 represent 1 SD and 2 SD, respectively. In addition, as the Q-Q plot shows a linear shape, the sample follows a Gaussian distribution.

Figure 2 shows dAOD analyzed for each satellite product, for the analysis period from April 2018 to March 2019, excluding the EMerGe campaign. In the Q-Q plot, the overall linear relationship is well represented within 1 SD. There is no linear relationship between 1 SD (black solid line) and 2 SD (black dotted line), but soon again appears in a linear relationship.

To minimize the effect of outliers in this process, data beyond 2 SD were excluded and applied differently according to NDVI and time. Data beyond 2 SD of dAOD were excluded to prevent a change in bias trends due to AOD errors caused by cloud shadows and pixels contaminated by clouds. Bias correction values are provided in Figure 3 where Gaussian center is calculated differently for NDVI, time, and respective satellite products, through the Gaussian fitting of the dAODs. Through this process of shifting the obtained Gaussian center values to match the 0 in bias, the systematic bias of the algorithms was corrected. This process was performed before applying the MLE method, which allows compensation for systematic bias that is difficult to obtain directly in MLE.

3.5 Evaluation of aerosol products during two field campaigns

The performance of fused products was analyzed in two field campaigns: the KORUS-AQ of 1 May 2016 to 12 Jun 2016 (<https://www-air.larc.nasa.gov/missions/korus-aq/>), and the EMerGe of 12 Mar 2018 to 8 Apr 2018 (<https://www.halo.dlr.de/science/missions/emerge/emerge.html>). KORUS-AQ was an international multi-organization mission to observe air quality across the Korean Peninsula and surrounding waters, led by the US National Aeronautics and Space Administration (NASA) and the Korean National Institute of Environmental Research (NIER). EMerGe aimed to investigate experimentally the patterns of atmospheric transport and transformation of pollution plumes originating from Eurasia, tropical and subtropical Asian megacities, and other major population centers. GEO satellite data played an important role in these campaigns; e.g., data assimilation for chemical transport models and tracking aerosol plumes (Saide et al., 2014, 2010; Pang et al., 2018). Here, we applied satellite-derived GOCI and AHI AODs, with a spatial resolution of 6 km × 6 km, and temporal resolutions of 1 hour and 10 minutes, respectively.

서식 지정함: 글꼴: 12 pt

삭제함: et al.,

삭제함: 3

삭제함: AOD differences with respect to AERONET/SONET data (삭제함:)

삭제함:

삭제함: ,

삭제함: ,

삭제함: by

삭제함: was selected

삭제함: The error distributions of AMR, AESR, GV1, and GV2 used here also follow a Gaussian distribution, with dAOD during the KORUS-AQ and EMerGe campaigns being as shown in Figure 1. ...

삭제함: Table

삭제함: .

삭제함: Figure 3

삭제함: and the Gaussian center is calculated

삭제함: It goes t

삭제함: a

삭제함: . This process serves to correct

서식 지정함: 글꼴: 14 pt

[1] 이동함(삽입)

삭제함: 2

삭제함: 3

삭제함: ; Saide et al., 2020

4. Results

Figure 4 (a) shows the average AOD of FM1 (MLE method with all products) during the KORUS-AQ period, and Figure 4 (b-k) shows the respective difference in the average AOD of AMR, AES, GV1, GV2, F1, F2, F3, F4, FM2, and FM3 with respect to FM1. The result of the comparison with the respective satellite product (Figure 4 (b-e)), shows different features. AMR shows a negative bias over the ocean but shows similar results to FM1 over land, while AES shows a different tendency in northern and southern China. GV1 tends to show opposite pattern to AES, and GV2 shows positive bias over the ocean and results in similar pattern to FM1 over the land. In the west of the Korean peninsula, AES AOD is overestimated compared to FM1. Although the AES algorithm considers the fraction of urbanization, there is still a tendency to overestimate AODs. The main reason why AES results show different patterns is the different estimation process of the land surface reflectance from that of other products.

On the other hand, in GV1, the AOD over the Manchurian region is overestimated. This is because the aerosol signal is small over bright surface, making it difficult to retrieve aerosol properties. These features tends to be alleviated in GV2, where the surface reflectance and cloud removal process were improved. Also, the difference was the least for the F1 result that differs only in the fusion method under the same configuration as FM1, and the F4 result (AMR, AES, and GV2) showed similar results. F3 and FM3, fusion products using AHI only, retain relatively strong AES features, thus their differences from FM1 (Figure 4 (h) and (k)) showing similar pattern as AES cases in Figure 4 (c).

Figure 5 shows the same result as Figure 4 except for the EMerGe period. The AMR and AES overestimated AODs in northern China, which is thought to be the snow contaminated pixel. The EMerGe period was in March-April, when northern China is more covered by snow compared to the KORUS-AQ period in May-June. On the other hand, for GV1 and GV2, the effect of overestimation with snow contaminated pixel is relatively small, as their snow masking is well performed. However, for the KORUS-AQ period, it seems that the GV1's overestimation of AOD in northern China still remains. FM1, the MLE product of F1, showed the most similar results naturally, followed by F4. However, since this analysis (Figure 4 and 5) is a fusion between the three MRM results and one ESR result, the average field difference is naturally the largest in AES which uses ESR method. For the characteristics of the average AOD for the two campaign period, high AODs during the KORUS-AQ period were found in eastern China, and Hokkaido as wildfires from Russia were transported to Hokkaido (Lee et al., 2019). Meanwhile, during the EMerGe period, high AOD is shown over the Yellow sea as aerosols were transported from China to the Korean peninsula through the west coast, contrary to the KORUS-AQ period. Overall, the average AODs for the EMerGe are less smooth than those of the KORUS-AQ period. This is because the EMerGe period was shorter than that of the KORUS-AQ, and the retrieval accuracy was lower due to the bright surface.

The Gangneung-Wonju National University site (Gangneung-WNU; 128.87°E, 37.77°N) lies on the eastern side of the Korean Peninsula and it is one of the regions with low aerosol loadings. The AOD frequency distribution generally follows a log-normal distribution, and it is important to estimate low

서식 지정함: 글꼴: 12 pt

삭제함: AOD products retrieved by each satellite instrument, ensemble-mean products, and the fusion products of the MLE method, are shown in Figure 2 for the KORUS-AQ period and in Figure 3 for the EMerGe period. The AOD fusion products (Figure 2a-d) tends to indicate higher AODs on the western side of the Korean Peninsula than the eastern side, and high AODs in Hokkaido, Japan. The same trends are observed over China with high AODs, where the AER product shows the highest values, and the respective satellite products display similar patterns. Large differences are evident in southern Tibet and the Taklamakan desert (Figure 2a, b) as a result of the error in the ESR method caused by unreliable surface reflectance over bright surfaces resulting in overestimation of AOD, as reported in previous studies (Levy et al., 2013; Gupta et al., 2016). The aerosol spatial distribution (Figure 2e-h) is similar in the different satellite products, and smooth overall. High AODs are noticeable over Shanghai, Hong Kong, and Hanoi (Figure 2g), consistent with the results of previous studies that reported high concentrations of surface particulate matter in urban regions. MLE results (Figure 2i-k) are similar to the ensemble-mean products....

삭제함: of the KORUS-AQ period ...f FM1 (MLE method with all)

삭제함: the bright surface, making it hard...ifficult to retrieve ... [2]

삭제함: .

삭제함: a difference from FM1

삭제함: .

삭제함: isshows the same result as Figure 4 except for the EMerGe [3]

삭제함:

삭제함: As for the characteristics of the average AOD of...or ... [4]

삭제함: due to the snow cover

삭제함: during the KORUS-AQ period, and ... [5]

삭제함: in

삭제함: , showing a high AOD distribution in ... [6]

삭제함: Results for the EMerGe campaign (Figure 3) are similar to those in Figure 2, but with higher AODs in northwestern Japan, Hokkaido, and northern Russia (particularly in Figure 3b). The AMR product (Figure 3a, c, d) indicates small errors, but snow masking needs to be improved. It also shows high AODs over the Yellow Sea, indicating that aerosols were transported from China during the EMerGe campaign. For the ensemble mean AODs, each satellite-derived product complements each other, reduced the scattered distribution in the lower AOD region to improve overall accuracy which can be compared and demonstrated well at sites with low aerosol loadings in particular.

AOD levels exactly to increase its accuracy. Therefore, we evaluated whether the fused products were improved at low AODs. A time-series comparison of different satellite AOD products with AERONET (on a logarithmic scale) is shown in Figure 6 for the Gangneung-WNU site without high AOD events, where most point AERONET AODs at 550 nm were < 1 during the KORUS-AQ campaign. Time-series data from ground instrument, AMR, AES, GV1, and GV2 products are shown in Figure 6 (a), where black filled circles represent AERONET AOD as ground-truth data, and satellite-derived AODs (in different colors) show similar variabilities. AMR, GV1, and GV2 products based on the MRM generally exhibit negative biases, with AES AODs being higher than other products. Ensemble-mean and MLE results are presented in Figure 6 (b) and (c), respectively, and show better agreement with the AERONET AOD than individual satellite AOD. This can also be seen from the dAOD indicated as solid line in Figure 6, where errors become smaller by going through the fusion process.

MLE results, which consider pixel-level uncertainties (in contrast to ensemble means), are superior in following the variability of ground-based AERONET observations, even at low AODs. The MLE products were implemented in a way to improve accuracy for the low AOD region more critically than in the high AOD region by systematic bias correction. Surface reflectance estimated by the MRM is affected by BAOD, and AOD thus shows a negative bias. On the other hand, the AER uses TOA reflectance at 1.6 μm wavelength to estimate surface reflectance and is therefore less affected by BAOD, and shows higher AOD than AMR and the two GOCI AODs. Furthermore, AOD retrieval over vegetated areas is more accurate with the ESR method. This result is consistent with previous studies of aerosol retrieval in the VIS region (Levy et al., 2013; Gupta et al., 2019; Hsu et al., 2019).

- 삭제함: and MLE
- 삭제함: 4
- 삭제함: 4a
- 삭제함: display
- 삭제함: outputs
- 삭제함: 4b
- 삭제함: s
- 삭제함: in
- 삭제함: (
- 삭제함:)
- 삭제함: and
- 삭제함: the
- 삭제함: s

5. Error estimation and validation against AERONET

For validation and error estimation, AERONET aerosol products were used for ground truth. AERONET offers freely available spectral AOD measurements every 15 min (or less) at numerous monitoring sites worldwide, with an uncertainty of 1%–2% under cloudless conditions (Smirnov et al., 2000; Holben et al., 2001). Newly updated AERONET Version 3 Level 2.0 AOPs with additional cloud screening and quality control were selected for validation purposes (Giles et al., 2019). The number of AERONET sites used for validation in this study, was 78 and 42 during the KORUS-AQ campaign, and 68 and 27 during the EMERGe campaign, for AHI and GOCI, respectively.

- 서식 지정함: 글꼴: 12 pt
- 삭제함: and SONET
- 삭제함: /SONET
- 삭제함: /SONET
- 삭제함:
- 삭제함: /SONET
- 서식 지정함: 글꼴: 12 pt
- 삭제함: and SONET
- 삭제함: /SONET
- 삭제함: /SONET
- 삭제함: /SONET
- 삭제함:
- 삭제함: 5
- 삭제함: 1
- 삭제함: 5
- 삭제함: 1
- 삭제함: 0
- 삭제함: 49
- 삭제함: 0

5.1 Validation with AERONET

Spatio-temporal correlation between satellite-derived AOD and AERONET AOD involved data averaged over all satellite pixels within a 25 km radius of the AERONET site, and AERONET AOD averaged over ±30 minutes from the satellite observation time. As validation metrics, Pearson's correlation coefficient, mean absolute error (MAE), median bias error (MBE), and the fraction (%) within the expected error (EE) were applied. The MODIS DT algorithm provided EE as $\pm 0.05 \pm 0.15 \times$ AOD (Levy et al., 2010). Results of the comparison with AERONET during the KORUS-AQ are shown in Figure 7, the EE values of AER, AES, G1, and GV2 were 53.2%, 58.0%, 52.2%, and 50.3%,

655 respectively. Fused products have EE values of up to 73.3%, much higher than the respective satellite product. In terms of RMSE, all of the fusion products without F3 and FM3 (validation over a broader area) have a value of 0.128, lower than the minimum value of various satellite products (0.153). Figure 7 (g) and (k) shows relatively scattered patterns compared with other fusion products because they show data fused with only AHI products. EE values for all AERONET products used for validation are shown in Figure 8, where AHI covers a broader area than GOCI. The accuracy is low over northern India and the Indochina Peninsula. However, EE values after fusion (Figure 8 (g, k)) are higher than those of the respective satellite product. The fused results (Figure 8 (g, k)) of two AHI products display high EE values within the domains of GOCI and other fusion products. The scattered fusion results based on two AHI products (Figure 7) can thus be attributed to issues at these particular sites, rather than to the satellite products themselves. Results of the comparative validation with AERONET during the EMerGe campaign (Figure 9) indicate that, overall, fusion products improve the statistical metrics, as in the KORUS-AQ case. The validation result for each satellite product shows that the maximum value of EE is 63.4%–68.0% after fusion. Thus, the EE increases as other statistics improve, including an RMSE decrease from 0.162 to 0.149. However, despite the MLE fusion (FM1-3) with bias correction using the Gaussian center values, MBE shows a rather poor result. This is because the Gaussian center value used for error correction does not work properly during the EMerGe campaign. Low NDVI in summer is generally seen for bright surfaces such as deserts, but low NDVIs are present in many areas, other than deserts during the EMerGe campaign period. To improve this, it is desirable to use seasonal Gaussian center values.

675 As in the KORUS-AQ campaign, the validation results for the two AHI products and the fusion products based on AHI AODs only are inferior to the results for the fusion products based on GOCI AODs. This is because the validation was performed over wider areas, and problems were noted at specific sites. The fused results showed improved accuracy not only in terms of EE but also in statistical metrics such as RSME, MBE, and MAE. Results for the EMerGe campaign are shown in Figure 10. During that campaign, validation results over brighter surfaces in northern India and the Indochina Peninsula show reduced accuracy, but fusion results show consistently higher EE values than individual satellite products.

680 5.2 Error estimation

685 Differences between satellite products and AERONET, dAOD values were analyzed on the basis of NDVI values and observation times (Figure 11). Figure 11 (a) and d shows the respective satellite products, Figure 11 (b) and (c) the ensemble-mean product, and Figure 11 (e) and (f) the MLE fusion results, with each filled circle representing the mean of 800 and 600 collocated data points sorted in terms of NDVI for the KORUS-AQ and the EMerGe campaigns, respectively. Figure 11a shows different biases for each satellite product, with AMR and GV1 being negative, AES positive, and GV2 converging to almost zero. The errors are close to zero for both the ensemble-mean and MLE products as a result of the fusion process. During the EMerGe campaign (right column, Figure 11), the two AHI and two GOCI products show negative biases, and even the ensemble-mean results have negative biases. 690 The ensemble mean does not include any bias correction, meaning that the error characteristics of each

- 삭제함: and MLE products
- 삭제함: 1
- 삭제함: 9
- 삭제함: the
- 삭제함: with
- 삭제함: 131
- 삭제함: 161
- 삭제함: 5g
- 삭제함: 6
- 삭제함: 6
- 삭제함: 6g
- 삭제함: only
- 삭제함: 5
- 삭제함: 7
- 삭제함: 1
- 삭제함: 5
- 삭제함: 9
- 삭제함: 7
- 삭제함: 6
- 삭제함: ,
- 삭제함: and an MBE decrease to zero.
- 삭제함: that performs
- 삭제함: significantly
- 삭제함: on
- 삭제함: during the EMerGe campaign.
- 삭제함: not
- 삭제함: just
- 삭제함: would be
- 삭제함: 8
- 서식 지정함: 글꼴: 12 pt
- 삭제함: 9
- 삭제함: 9a
- 삭제함: 9b
- 삭제함: 9c
- 삭제함: 9a
- 삭제함: 9

original satellite product are intact. The MLE products display improved biases in terms of NDVI, which are close to zero because the bias was corrected for in the MLE process.

The **median** bias of the AOD products over the observation time was analyzed as shown in Figure 12 where the left column represents the KORUS-AQ and the right column the EMeRGe campaign, with filled circles representing **median** values, and the error bar being ± 1 SD. As in **the KORUS-AQ campaign**, the AMR **shows** a generally negative bias, as in the all-time results, and a negative bias also exists in each time zone. However, the AES shows a positive bias. In the GOCI case, positive and negative biases appear differently according to time zones. In the EMeRGe period, the two AHI results have large error ranges. GEO satellites perform observations over a specific area with a fixed viewing zenith-angle and retrieve AOPs by solar reflectance, which means that a specific site has different local time depending on its longitude for a given satellite image. Furthermore, there are fewer data for the EMeRGe period than the KORUS-AQ period, and data for northern India and the Indochina Peninsula, which have low accuracy, are included in the data for 0100–0300 UTC, indicating large errors. In the KORUS-AQ period, the data fraction for a specific site is not as large as in the EMeRGe period, so this problem does not arise.

Taylor diagrams for accuracy evaluation of AOD data fusion products are shown in Figure 13. The Taylor diagram is a graphic summary of how closely satellite retrievals match observations. Here, match-up values were respective and fusion AOD products, and the matching up data were AERONET AOD. Correlation coefficient, SD, RSME, and EE values were used as the matching criteria. The correlation coefficient is shown in green (Figure 13) with a polar angle, the SD is shown in the radial distance on the black x- and y-axes, and RMSE is the proportional cyan circle from the “AERONET” point on the x-axis. The EE value, which can evaluate the stability of AODs, is shown for each color. AMR, AES, **GV1, GV2, F1, F2, F3, F4, FM1, FM2, and FM3** are indicated by **different symbol**, respectively.

Correlation coefficients are all around 0.8–0.9 with no significant differences for respective and fusion AODs. However, results after fusion show slightly better than respective satellite product accuracy in terms of SD, RMSE, and EE values.

Standard deviation values indicate that products that lie outside the purple dotted half-circle are larger than the SD of AERONET. In the AHI case, the SD appears smaller than GOCI values because it tends to underestimate values at high AOD. Similarly, RMSE values are lower after fusion.

The EMeRGe period was from March to April, when the surface is brighter in East Asia than during the KORUS-AQ period of May to June. The accuracy during the EMeRGe period is therefore similar to or slightly poorer than that of the KORUS-AQ period. The correlation coefficient shows similar values, but the SD, RMSE, and EE values are slightly lower. Again, the accuracy of the validation metrics is improved by fusion.

The error analysis indicates that the results after fusion are more accurate than the results obtained using individual satellite product, and accuracy was slightly better during KORUS-AQ than EMeRGe because more data points were considered. **Also, the surface was relatively dark during the KORUS-AQ period, thus reduced errors for aerosol retrieval than during the EMeRGe period.**

삭제함: mean

삭제함: 10

삭제함: , as in Figure 9,

삭제함: mean

삭제함: Figure 9

삭제함: displays

삭제함: 11

삭제함: 11

삭제함: All open symbols represent the results of selecting only the same collocation site as GOCI, and the filled symbols are comparative validations of all sites. GV1, GV2, ...

삭제함:

삭제함: square, circle, diamond, star, top half circle, lower half circle, left half circle, right half circle, triangle, right-pointing triangle, and left-pointing triangle diamond, star, square, circle, top half-circle,

삭제함: diamond, star, square, circle, top half-circle, lower half-circle, left half-circle, right half-circle, down-pointing triangle, right-pointing triangle, and left-pointing triangle shapes, respectively.

삭제함: The filled symbols cover a large area, so sites with poor accuracy are reflected in correlations, SD, RMSE, and EE values. ...

삭제함: However, the results of AMR and AER included in the GOCI observation area show better accuracy than the GOCI, with statistical metrics similar to those of the fusion products....

삭제함: i

삭제함: so

삭제함: is better

5.3 Accuracy evaluation for AHI products of GOCI domain

In this section, the accuracy of AHI products in the GOCI domain was evaluated. Table 2 shows all sites and co-located sites with GOCI for AMR, AES, F3, and FM3, where values exist for a wide area, and summarizes them for the KORUS-AQ and the EMERGe periods. First, during the KORUS-AQ period, it can be seen that the number of collocated data has decreased by about 2000 points. By reducing the validation area, R, RMSE, MBE, and %EE were improved. RMSE is 0.150 and 0.145, which is better than 0.153 and 0.176 of GV1 and GV2, and there is a difference of more than 10% in %EE. Likewise, the results of fusion products are also improved.

However, there is a slightly different trend for the EMERGe period. First of all, by reducing the area, the percentage of reduced points is more than 60%, which is more than the 30% for the KORUS-AQ period. In existing AMR and AES products, the statistical value tends to increase as the area becomes smaller. However, the fusion product's accuracy is rather decreased for the GOCI coverage. For AMR and AES, MBE and RMSE are similar to or better than GV1 and GV2, and %EE are higher than GV1 and GV2. However, in contrast to the KORUS-AQ period, the bias characteristics of AMR and AES are also negative, so the accuracy of F3 is inferior to the existing products. Meanwhile, the decrease in the accuracy of the FM3 product can be explained by difficulty to obtain accurate statistics due to higher weight in other areas beyond GOCI domain.

6. Summary and conclusion

Various aerosol algorithms have been developed based on two different GEO satellites, AHI, and GOCI. Retrieved AOD data have advantages and disadvantages, depending on the concept of the algorithm and surface-reflectance estimations. In this study, four aerosol products (GV1, GV2, AMR, and AES) were used to construct ensemble-mean and MLE products. Based on the ensemble mean, this study presented fusion products taking advantage of overlap region, accuracy, and near-real-time processing, as well as MLE products including pixel-level errors. Bias corrections for different times were performed while considering pixel-level errors, and the synergy of fusion between GEO satellites demonstrated.

Validation with the AERONET confirmed that consideration of pixel-level uncertainty improved the accuracy of MLE products. The accuracy after fusion was better than that of individual satellite product. The %EE of each satellite-derived product during the KORUS-AQ was 53.2%, 58.0%, 52.2%, and 50.3% in AMR, AES, GV1, and GV2; and the RMSE was 0.180, 0.201, 0.153, and 0.176, respectively. After the ensemble-mean process, the EE of F1, F2, F3, and F4 increased to 67.8%, 72.3%, 63.5%, and 73.3%, respectively. FM1, FM2, and FM3, which are results of MLE fusion, had %EE values of 71.5%, 65.6%, and 65.0%, with RMSE values of 0.131, 0.148, and 0.161, respectively, better than the respective satellite product. Similarly, the EMERGe period displayed better statistical values after fusion, with EE and RMSE values of 68.0% and 0.149, respectively. To provide optimized AOD products for East Asia, NDVI and time-dependent errors have been reduced. The ensemble mean and MLE fusion results show

서식 지정함: 글꼴: 12 pt

서식 있음: 제목 2

삭제함: in

삭제함: s. HoweverBut... the fusion product's accuracy is rather... [7]

서식 지정함: 글꼴: 12 pt

삭제함: 12%, 58.05..., 521...26..., and 5049...30... in AMR, AE[8]

better accuracy, and both show consistent results, indicating that there is no significant difference from the mean AOD in Figures 4(f) and 5 (f).

삭제함: similar

삭제함: in the difference

875 However, since both satellite algorithms retrieved AOPs through VIS channels, there remains an issue of reduced accuracy over brighter surfaces, with AOP retrieval in the VIS channel being more accurate over dark surfaces, and with results being more accurate during the KORUS-AQ period than the EMERGe period. The fusion products improved the accuracy of satellite products, and MLE products, also improved the accuracy by taking into account pixel-based errors based on long-term data analysis.

삭제함: further

880 The method applied in this study could be used for AOD fusion of GEO data, such as AMI onboard GK-2A, and GOCI-2 and GEMS onboard GK-2B. Furthermore, it is possible to retrieve AOPs other than AOD using multi-angle, multi-channel (UV, VIS, and IR) observations with GK-2A and 2B.

삭제함:

885 Code and data availability.

The aerosol products data from AHI and GOCI are available on request from the corresponding author (jkim2@yonsei.ac.kr).

890 Author contributions.

HL, SG and JK designed the experiment. HL and SG carried out the data processing. MC, SL, and YK provided support on satellite data. HL wrote the manuscript with contributions from co-authors. JK reviewed and edited the article. JK and CK provided support and supervision. All authors analyzed the measurement data and prepared the article with contributions from all co-authors.

Competing interests.

The authors declare that they have no conflict of interest.

900

Acknowledgements

We thank all principal investigators and their staff for establishing and maintaining the AERONET sites used in this investigation. This subject is supported by Korea Ministry of Environment (MOE) as "Public Technology Program based on Environmental Policy (2017000160001)". This work was also supported by a grant from the National Institute of Environment Research (NIER), funded by the Ministry of Environment (MOE) of the Republic of Korea (NIER-2020-01-02-007). This research was also supported by the National Strategic Project-Fine particle of the National Research Foundation of Korea (NRF) funded by the Ministry of Science and ICT (MSIT), the Ministry of Environment (ME), and the Ministry of Health and Welfare (MOHW) (NRF-2017M3D8A1092022). We thank all members of the KORUS-AQ science team for their contributions to the field study and the data processing (doi:10.5067/Suborbital/KORUSAQ/DATA01).

910

References

920 Bernard, E., Moulin, C., Ramon, D., Jolivet, D., Riedi, J., and Nicolas, J. M.: Description and validation of an AOT product over land at the 0.6 μm channel of the SEVIRI sensor onboard MSG, *Atmospheric Measurement Techniques*, 4, 2543-2565, 2011.

Bessho, K., Date, K., Hayashi, M., Ikeda, A., Imai, T., Inoue, H., Kumagai, Y., Miyakawa, T., Murata, H., Ohno, T., Okuyama, A., Oyama, R., Sasaki, Y., Shimazu, Y., Shimoji, K., Sumida, Y., Suzuki, M., Taniguchi, H., Tsuchiyama, H., Uesawa, D., Yokota, H., and Yoshida, R.: An Introduction to Himawari-8/9—Japan’s New-Generation Geostationary Meteorological Satellites, *Journal of the Meteorological Society of Japan. Ser. II*, 94, 151-183, 2016.

925 Bilal, M., Nichol, J. E., and Wang, L.: New customized methods for improvement of the MODIS C6 Dark Target and Deep Blue merged aerosol product, *Remote Sensing of Environment*, 197, 115-124, 2017.

Chatterjee, A., Michalak, A. M., Kahn, R. A., Paradise, S. R., Braverman, A. J., and Miller, C. E.: A geostatistical data fusion technique for merging remote sensing and ground-based observations of aerosol optical thickness, *Journal of Geophysical Research*, 115, 2010.

930 Cho, Hi K., Jeong, M. J., Kim, J., Kim, Y. J.: Dependence of diffuse photosynthetically active solar irradiance on total optical depth, *Journal of Geophysical Research*, 108, D9, 4267, 4-1–4-10, 2003.

935 Choi, J.-K., Park, Y. J., Ahn, J. H., Lim, H.-S., Eom, J., and Ryu, J.-H.: GOCI, the world's first geostationary ocean color observation satellite, for the monitoring of temporal variability in coastal water turbidity, *Journal of Geophysical Research: Oceans*, 117, C9, 2012.

Choi, M., Kim, J., Lee, J., Kim, M., Park, Y.-J., Jeong, U., Kim, W., Hong, H., Holben, B. N., Eck, T. F., Song, C. H., Lim, J.-H., and Song, C.-K.: GOCI Yonsei Aerosol Retrieval (YAER) algorithm and validation during the DRAGON-NE Asia 2012 campaign, *Atmos. Meas. Tech.*, 9, 1377-1398, 2016.

940 Choi, M., Kim, J., Lee, J., Kim, M., Park, Y.-J., Holben, B., Eck, T. F., Li, Z., and Song, C. H.: GOCI Yonsei aerosol retrieval version 2 products: an improved algorithm and error analysis with uncertainty estimation from 5-year validation over East Asia, *Atmospheric Measurement Techniques*, 11, 385-408, 2018.

Cox, C.: Statistics of the sea surface derived from sun glitter, *J. Marine Research*, 13, 198-227, 1954.

945 Fukuda, S., Nakajima, T., Takenaka, H., Higurashi, A., Kikuchi, N., Nakajima, T. Y., and Ishida, H.: New approaches to removing cloud shadows and evaluating the 380 nm surface reflectance for improved aerosol optical thickness retrievals from the GOSAT/TANSO-Cloud and Aerosol Imager, *Journal of Geophysical Research: Atmospheres*, 118, 13,520-513,531, 2013.

Garay, M. J., Kalashnikova, O. V., and Bull, M. A.: Development and assessment of a higher-spatial-resolution (4.4 km) MISR aerosol optical depth product using AERONET-DRAGON data, *Atmospheric Chemistry and Physics*, 17, 5095-5106, 2017.

950 Garay, M. J., Witek, M. L., Kahn, R. A., Seidel, F. C., Limbacher, J. A., Bull, M. A., Diner, D. J., Hansen, E. G., Kalashnikova, O. V., Lee, H., Nastan, A. M., and Yu, Y.: Introducing the 4.4Ékm spatial resolution Multi-Angle Imaging SpectroRadiometer (MISR) aerosol product, *Atmospheric Measurement Techniques*, 13, 593-628, 2020.

- 955 Giles, D. M., Sinyuk, A., Sorokin, M. S., Schafer, J. S., Smirnov, A., Slutsker, I., Eck, T. F., Holben, B. N., Lewis, J., Campbell, J., Welton, E. J., Korkin, S., and Lyapustin, A.: Advancements in the Aerosol Robotic Network (AERONET) Version 3 Database – Automated Near Real-Time Quality Control Algorithm with Improved Cloud Screening for Sun Photometer Aerosol Optical Depth (AOD) Measurements, *Atmos. Meas. Tech. Discuss.*, doi: <https://doi.org/10.5194/amt-2018-272>, 2018. 2018.
- 960 [Go, S., Kim, J., Park, S. S., Kim, M., Lim, H., Kim, J.-Y., Lee, D.-W., and Im, J.: Synergistic Use of Hyperspectral UV-Visible OMI and Broadband Meteorological Imager MODIS Data for a Merged Aerosol Product, *Remote Sensing*, 12, 2020.](#)
- ▲ Gupta, P., Patadia, F., and Christopher, S. A.: Multisensor Data Product Fusion for Aerosol Research, *IEEE Transactions on Geoscience and Remote Sensing*, 46, 1407-1415, 2008.
- 965 Gupta, P., Levy, R. C., Mattoo, S., Remer, L. A., and Munchak, L. A.: A surface reflectance scheme for retrieving aerosol optical depth over urban surfaces in MODIS Dark Target retrieval algorithm, *Atmospheric Measurement Techniques*, 9, 3293-3308, 2016.
- Gupta, P., Levy, R. C., Mattoo, S., Remer, L. A., Holz, R. E., and Heidinger, A. K.: Applying the Dark Target aerosol algorithm with Advanced Himawari Imager observations during the KORUS-AQ field campaign, 2019. 2019.
- 970 Herman, J., Bhartia, P., Torres, O., Hsu, C., Sefstor, C., and Celarier, E.: Global distribution of UV-absorbing aerosols from Nimbus 7/TOMS data, *Journal of Geophysical Research: Atmospheres*, 102, 16911-16922, 1997.
- Holben, B. N., Tanre, D., Smirnov, A., Eck, T., Slutsker, I., Abuhassan, N., Newcomb, W., Schafer, J., Chatenet, B., and Lavenu, F. J. J. o. G. R. A.: An emerging ground-based aerosol climatology: Aerosol optical depth from AERONET, 106, 12067-12097, 2001.
- 975 Hsu, N. C., Tsay, S.-C., King, M. D., Herman, J. R. J. I. T. o. G., and Sensing, R.: Aerosol properties over bright-reflecting source regions, 42, 557-569, 2004.
- Hsu, N., Jeong, M. J., Bettenhausen, C., Sayer, A., Hansell, R., Sefstor, C., Huang, J., and Tsay, S. C.: Enhanced Deep Blue aerosol retrieval algorithm: The second generation, *Journal of Geophysical Research: Atmospheres*, 118, 9296-9315, 2013.
- Hsu, N., Lee, J., Sayer, A., Kim, W., Bettenhausen, C., and Tsay, S. C. J. J. o. G. R. A.: VIIRS Deep Blue aerosol products over land: Extending the EOS long-term aerosol data records, 124, 4026-4053, 2019.
- 980 Jackson, J. M., Liu, H., Laszlo, I., Kondragunta, S., Remer, L. A., Huang, J., and Huang, H.-C.: Suomi-NPP VIIRS aerosol algorithms and data products, *Journal of Geophysical Research: Atmospheres*, 118, 612,673-612,689, 2013.
- Kikuchi, M., Murakami, H., Suzuki, K., Nagao, T. M., and Higurashi, A.: Improved Hourly Estimates of Aerosol Optical Thickness Using Spatiotemporal Variability Derived From Himawari-8 Geostationary Satellite, *IEEE Transactions on Geoscience and Remote Sensing*, 56, 3442-3455, 2018.
- 985 Kim, J., Lee, J., Lee, H. C., Higurashi, A., Takemura, T., and Song, C. H., Consistency of the aerosol type classification from satellite remote sensing during the Atmospheric Brown Cloud–East Asia Regional Experiment campaign, *J. Geophys. Res.*, 112, D22S33, doi:10.1029/2006JD008201, 2007.
- Kim, J., Yoon, J. M., Ahn, M. H., Sohn, B. J., and Lim, H. S.: Retrieving aerosol optical depth using visible and mid-IR channels from geostationary satellite MTSAT-1R, *International Journal of Remote Sensing*, 29, 6181-6192, 2008.
- 990 Kim, J., Kim, M., and Choi, M.: Monitoring aerosol properties in east Asia from geostationary orbit: GOCI, MI and GEMS. In: *Air Pollution in Eastern Asia: An Integrated Perspective*, Springer, 2017.

서식 지정법: 글꼴: (영어) Times New Roman, 12 pt, 굵게
 서식 있음: 표준

995 Kim, J., Jeong, U., Ahn, M.-H., Kim, J. H., Park, R. J., Lee, H., Song, C. H., Choi, Y.-S., Lee, K.-H., Yoo, J.-M., Jeong, M.-J., Park, S. K., Lee, K.-M., Song, C.-K., Kim, S.-W., Kim, Y. J., Kim, S.-W., Kim, M., Go, S., Liu, X., Chance, K., Chan Miller, C., Al-Saadi, J., Veiheilmann, B., Bhartia, P. K., Torres, O., Abad, G. G., Haffner, D. P., Ko, D. H., Lee, S. H., Woo, J.-H., Chong, H., Park, S. S., Nicks, D., Choi, W. J., Moon, K.-J., Cho, A., Yoon, J., Kim, S.-k., Hong, H., Lee, K., Lee, H., Lee, S., Choi, M., Veeckind, P., Levelt, P. F., Edwards, D. P., Kang, M., Eo, M., Bak, J., Baek, K., Kwon, H.-A., Yang, J., Park, J., Han, K. M., Kim, B.-R., Shin, H.-W., Choi, H., Lee, E., Chong, J., Cha, Y., Koo, J.-H., Irie, H., Hayashida, S., Kasai, Y., Kanaya, Y., Liu, C., Lin, J., Crawford, J. H., Carmichael, G. R., Newchurch, M. J., Lefer, B. L., Herman, J. R., Swap, R. J., Lau, A. K. H., Kurosu, T. P., Jaross, G., Ahlers, B., Dobber, M., McElroy, C. T., and Choi, Y.: New Era of Air Quality Monitoring from Space: Geostationary Environment Monitoring Spectrometer (GEMS), *Bulletin of the American Meteorological Society*, 101, E1-E22, 2020.

Kim, M., Kim, J., Wong, M. S., Yoon, J., Lee, J., Wu, D., Chan, P. W., Nichol, J. E., Chung, C.-Y., and Ou, M.-L.: Improvement of aerosol optical depth retrieval over Hong Kong from a geostationary meteorological satellite using critical reflectance with background optical depth correction, *Remote Sensing of Environment*, 142, 176-187, 2014.

005 Kim, M., Kim, J., Jeong, U., Kim, W., Hong, H., Holben, B., Eck, T. F., Lim, J. H., Song, C. K., Lee, S., and Chung, C. Y.: Aerosol optical properties derived from the DRAGON-NE Asia campaign, and implications for a single-channel algorithm to retrieve aerosol optical depth in spring from Meteorological Imager (MI) on-board the Communication, Ocean, and Meteorological Satellite (COMS), *Atmos. Chem. Phys.*, 16, 1789-1808, 2016.

010 Kim, M., Kim, S. H., Kim, W. V., Lee, Y. G., Kim, J., and Kafatos, M. C.: Assessment of Aerosol optical depth under background and polluted conditions using AERONET and VIIRS datasets, *Atmospheric Environment*, 245, 2021.
Knapp, K. R. J. o. G. R. A.: Quantification of aerosol signal in GOES 8 visible imagery over the United States, 107, AAC 4-1-AAC 4-11, 2002.

Knapp, K. R., Frouin, R., Kondragunta, S., and Prados, A.: Toward aerosol optical depth retrievals over land from GOES visible radiances: determining surface reflectance, *International Journal of Remote Sensing*, 26, 4097-4116, 2007.

015 Koelemeijer, R., De Haan, J., and Stammes, P.: A database of spectral surface reflectivity in the range 335–772 nm derived from 5.5 years of GOME observations, *Journal of Geophysical Research: Atmospheres*, 108, 2003.

Lee, J., Kim, J., Song, C. H., Ryu, J.-H., Ahn, Y.-H., and Song, C.: Algorithm for retrieval of aerosol optical properties over the ocean from the Geostationary Ocean Color Imager, *Remote Sensing of Environment*, 114, 1077-1088, 2010.

020 Lee, J., Kim, J., Yang, P., and Hsu, N. C.: Improvement of aerosol optical depth retrieval from MODIS spectral reflectance over the global ocean using new aerosol models archived from AERONET inversion data and tri-axial ellipsoidal dust database, *Atmospheric Chemistry and Physics*, 12, 7087-7102, 2012.

Levy, R. C., Remer, L. A., Kleidman, R. G., Mattoo, S., Ichoku, C., Kahn, R., and Eck, T. F.: Global evaluation of the Collection 5 MODIS dark-target aerosol products over land, *Atmospheric Chemistry and Physics*, 10, 10399-10420, 2010.

025 Levy, R. C., Mattoo, S., Munchak, L. A., Remer, L. A., Sayer, A. M., Patadia, F., and Hsu, N. C.: The Collection 6 MODIS aerosol products over land and ocean, *Atmospheric Measurement Techniques*, 6, 2989-3034, 2013.

Lee, S., Kim, M., Choi, M., Go, S., Kim, J., Kim, J.-H., Lim, H.-K., Jeong, U., Goo, T.-Y., Kuze, A., Shiomi, K., and Tatsuya, Y.: Aerosol Property Retrieval Algorithm over Northeast Asia from TANSO-CAI Measurements Onboard GOSAT, *Remote Sensing*, 9, 2017.

030 Lee, S., Kim, J., Choi, M., Hong, J., Lim, H., Eck, T. F., Holben, B. N., Ahn, J.-Y., Kim, J., and Koo, J.-H.: Analysis of long-range transboundary transport (LRTT) effect on Korean aerosol pollution during the KORUS-AQ campaign, *Atmospheric Environment*, 204, 53-67, 2019.

▲

서식 지정함: 글꼴: 10 pt, 영어(영국)

서식 있음: 표준

서식 지정함: 글꼴: 10 pt

삭제함: ←

서식 지정함: 글꼴: 10 pt, 영어(영국)

서식 있음: 표준

서식 지정함: 글꼴: (영어) Times New Roman, (한글) 바탕, 굵게, (한글) 한국어

- 035 Li, L., Shi, R., Zhang, L., Zhang, J., and Gao, W.: The data fusion of aerosol optical thickness using universal kriging and stepwise regression in East China, 2014, 922112.
- Lim, H., Choi, M., Kim, M., Kim, J., and Chan, P. W.: Retrieval and Validation of Aerosol Optical Properties Using Japanese Next Generation Meteorological Satellite, Himawari-8, Korean Journal of Remote Sensing, 32, 681-691, 2016.
- 040 Lim, H., Choi, M., Kim, J., Kasai, Y., and Chan, P.: AHI/Himawari-8 Yonsei Aerosol Retrieval (YAER): Algorithm, Validation and Merged Products, Remote Sens., 10, 2018.
- Lyapustin, A., Martonchik, J., Wang, Y., Laszlo, I., and Korkin, S.: Multiangle implementation of atmospheric correction (MAIAC): 1. Radiative transfer basis and look-up tables, Journal of Geophysical Research, 116, 2011a.
- Lyapustin, A., Wang, Y., Laszlo, I., Kahn, R., Korkin, S., Remer, L., Levy, R., and Reid, J. S.: Multiangle implementation of atmospheric correction (MAIAC): 2. Aerosol algorithm, Journal of Geophysical Research, 116, 2011b.
- 045 Lyapustin, A., Wang, Y., Korkin, S., and Huang, D.: MODIS Collection 6 MAIAC algorithm, Atmospheric Measurement Techniques, 11, 5741-5765, 2018.
- Mélin, F., Zibordi, G., and Djavidnia, S.: Development and validation of a technique for merging satellite derived aerosol optical depth from SeaWiFS and MODIS, Remote Sensing of Environment, 108, 436-450, 2007.
- Murakami, H.: Ocean color estimation by Himawari-8/AHI, 2016, 987810.
- 050 Negi, H. and Kokhanovsky, A. J. T. C.: Retrieval of snow albedo and grain size using reflectance measurements in Himalayan basin, 5, 203, 2011.
- Nguyen, H., Cressie, N., and Braverman, A.: Spatial Statistical Data Fusion for Remote Sensing Applications, Journal of the American Statistical Association, 107, 1004-1018, 2012.
- Nirala, M.: Technical Note: Multi-sensor data fusion of aerosol optical thickness, International Journal of Remote Sensing, 29, 2127-2136, 2008.
- Pang, J., Liu, Z., Wang, X., Bresch, J., Ban, J., Chen, D., and Kim, J.: Assimilating AOD retrievals from GOCI and VIIRS to forecast surface PM2.5 episodes over Eastern China, Atmospheric Environment, 179, 288-304, 2018.
- Remer, L. A., Kaufman, Y., Tanré, D., Mattoo, S., Chu, D., Martins, J. V., Li, R.-R., Ichoku, C., Levy, R., and Kleidman, R.: The MODIS aerosol algorithm, products, and validation, Journal of the atmospheric sciences, 62, 947-973, 2005.
- 060 Remer, L. A., Mattoo, S., Levy, R. C., and Munchak, L.: MODIS 3 km aerosol product: algorithm and global perspective, Atmospheric Measurement Techniques Discussions, 6, 69-112, 2013.
- Saide, P. E., Kim, J., Song, C. H., Choi, M., Cheng, Y., and Carmichael, G. R.: Assimilation of next generation geostationary aerosol optical depth retrievals to improve air quality simulations, Geophysical Research Letters, 41, 9188-9196, 2014.
- 065 Saide, P. E., Gao, M., Lu, Z., Goldberg, D., Streets, D. G., Woo, J.-H., Beyersdorf, A., Corr, C. A., Thornhill, K. L., Anderson, B., Hair, J. W., Nehrir, A. R., Diskin, G. S., Jimenez, J. L., Nault, B. A., Campuzano-Jost, P., Dibb, J., Heim, E., Lamb, K. D., Schwarz, J. P., Perring, A. E., Kim, J., Choi, M., Holben, B., Pfister, G., Hodzic, A., Carmichael, G. R., Emmons, L., and Crawford, J. H.: Understanding and improving model representation of aerosol optical properties for a Chinese haze event measured during KORUS-AQ, Atmospheric Chemistry and Physics, 20, 6455-6478, 2020.
- 070 Sayer, A. M., Hsu, N. C., Bettenhausen, C., and Jeong, M. J.: Validation and uncertainty estimates for MODIS Collection 6 "Deep Blue" aerosol data, Journal of Geophysical Research: Atmospheres, 118, 7864-7872, 2013.

서식 지정함: 글꼴: 10 pt

- Sayer, A., Munchak, L., Hsu, N., Levy, R., Bettenhausen, C., and Jeong, M. J.: MODIS Collection 6 aerosol products: Comparison between Aqua's e-Deep Blue, Dark Target, and "merged" data sets, and usage recommendations, *Journal of Geophysical Research: Atmospheres*, 119, 2014.
- 075 Sayer, A., Hsu, N., Lee, J., Bettenhausen, C., Kim, W., and Smirnov, A. J. J. o. G. R. A.: Satellite Ocean Aerosol Retrieval (SOAR) Algorithm Extension to S-NPP VIIRS as Part of the "Deep Blue" Aerosol Project, 123, 380-400, 2018.
- Sayer, A. M., Hsu, N. C., Lee, J., Kim, W. V., and Dutcher, S. T.: Validation, Stability, and Consistency of MODIS Collection 6.1 and VIIRS Version 1 Deep Blue Aerosol Data Over Land, *Journal of Geophysical Research: Atmospheres*, 124, 4658-4688, 2019.
- 080 Smirnov, A., Holben, B. N., Eck, T. F., Dubovik, O., and Slutsker, I.: Cloud screening and quality control algorithms for the AERONET data base, *Remote Sens. Environ.*, 73, 337-349, 2000.
- Stocker, T. F., Qin, D., Plattner, G.-K., Tignor, M., Allen, S. K., Boschung, J., Nauels, A., Xia, Y., Bex, B., and Midgley, B.: IPCC, 2013: climate change 2013: the physical science basis. Contribution of working group I to the fifth assessment report of the intergovernmental panel on climate change. Cambridge University Press, 2013.
- 085 Tang, Q., Bo, Y., and Zhu, Y.: Spatiotemporal fusion of multiple-satellite aerosol optical depth (AOD) products using Bayesian maximum entropy method, *Journal of Geophysical Research: Atmospheres*, 121, 4034-4048, 2016.
- Wang, J.: Geostationary satellite retrievals of aerosol optical thickness during ACE-Asia, *Journal of Geophysical Research*, 108, 2003.
- Wang, J., Brown, D. G., and Hammerling, D.: Geostatistical inverse modeling for super-resolution mapping of continuous spatial processes, *Remote Sensing of Environment*, 139, 205-215, 2013.
- 090 [Wei, J., Li, Z., Sun, L., Peng, Y., and Wang, L.: Improved merge schemes for MODIS Collection 6.1 Dark Target and Deep Blue combined aerosol products, *Atmospheric Environment*, 202, 315-327, 2019.](#) [Xie, Y., Xue, Y., Che, Y., Guang, J., Mei, L., Voorhis, D., Fan, C., She, L., Xu, H. J. I. T. o. G., and Sensing, R.: Ensemble of ESA/AATSR aerosol optical depth products based on the likelihood estimate method with uncertainties, 56, 997-1007, 2018.](#)
- 095 Xu, H., Guang, J., Xue, Y., De Leeuw, G., Che, Y., Guo, J., He, X., and Wang, T. J. A. E.: A consistent aerosol optical depth (AOD) dataset over mainland China by integration of several AOD products, 114, 48-56, 2015.
- Xue, Y., Xu, H., Mei, L., Guang, J., Guo, J., Li, Y., Hou, T., Li, C., Yang, L., He, X. J. A. C., and Discussions, P.: Merging aerosol optical depth data from multiple satellite missions to view agricultural biomass burning in Central and East China, 12, 10461-10492, 2012.
- 100 Yoon, J. M., Kim, J., Lee, J. H., Cho, H. K., Sohn, B.-J., and Ahn, M.-H. J. A.-P. J. o. A. S.: Retrieval of aerosol optical depth over East Asia from a geostationary satellite, MTSAT-1R, 43, 49-58, 2007.
- Yoshida, M., Kikuchi, M., Nagao, T. M., Murakami, H., Nomaki, T., and Higurashi, A.: Common Retrieval of Aerosol Properties for Imaging Satellite Sensors, *Journal of the Meteorological Society of Japan. Ser. II*, 96B, 193-209, 2018.
- 105 Zhong, G., Wang, X., Tani, H., Guo, M., Chittenden, A., Yin, S., Sun, Z., and Matsumura, S.: A Modified Aerosol Free Vegetation Index Algorithm for Aerosol Optical Depth Retrieval Using GOSAT TANSO-CAI Data, *Remote Sensing*, 8, 2016.

삭제함: Wei, J., Li, Z., Sun, L., Peng, Y., Zhang, Z., Li, Z., Su, T., Feng, L., Cai, Z., and Wu, H.: Evaluation and uncertainty estimate of next-generation geostationary meteorological Himawari-8/AHI aerosol products, *Sci Total Environ*, 692, 879-891, 2019. [↗](#)

삭제함: 7

삭제함: Yamada, K., Ishizaka, J., Yoo, S., Kim, H.-c., and Chiba, S.: Seasonal and interannual variability of sea surface chlorophyll a concentration in the Japan/East Sea (JES), *Progress in Oceanography*, 61, 193-211, 2004. [↗](#)

Table 1. Satellite dataset used for the fusion products.

<u>AOD type</u>	<u>F1</u>	<u>F2</u>	<u>F3</u>	<u>F4</u>	<u>FM1</u>	<u>FM2</u>	<u>FM3</u>
<u>AER</u>	Q	Q	Q	Q	Q	Q	Q
<u>AMR</u>	Q		Q	Q	Q		Q
<u>GV1</u>	Q				Q		
<u>GV2</u>	Q	Q			Q	Q	
<u>Remark</u>				<u>Without GV1 to check missing effect</u>	<u>MLE Products²</u>		
	<u>All available products</u>	<u>For NRT¹</u>	<u>AHI only for wider area</u>		<u>Same as F1</u>	<u>Same as F2</u>	<u>Same as F3</u>

120

¹ NRT: near real time; ² Maximum Likelihood Estimation

삭제함: AOD type ... [9]

서식 있는 표

삭제함: O

삭제함: O

삭제함: O

서식 있음: 줄 간격: 1줄

삭제함: O

삭제함: O

삭제함: O

삭제함: O

삭제함: O

서식 있음: 줄 간격: 1줄

삭제함: O

삭제함: O

삭제함: O

삭제함: O

서식 있음: 줄 간격: 1줄

삭제함: O

서식 있음: 줄 간격: 1줄

서식 있는 표

삭제함: O

삭제함: O

삭제함: O

삭제함: O

서식 있음: 줄 간격: 1줄

서식 지정함: 위 첨자

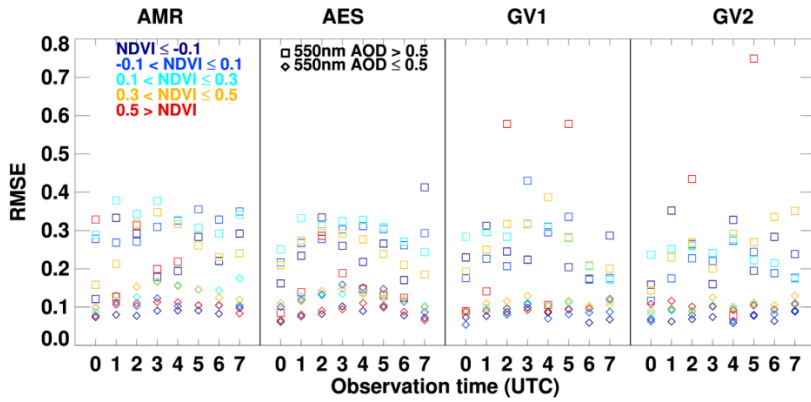
서식 있음: 들여쓰기: 왼쪽: 0.71 cm

서식 지정함: 글꼴: (영어)+본문(Times New Roman)

서식 지정함: 위 첨자

서식 지정함: 글꼴: (영어)+본문(Times New Roman), (한글)한국어

삭제함:페이지 나누기.....



145 Figure 1. RMSE according to NDVI (color), observation time, and satellite AODs (square and diamond represent AOD at 550nm greater and less equal than 0.5) during Apr. 2018 to Mar. 2019 excluding EMeRGe campaign.

서식 지정함: 글꼴: 10 pt, 굵게 없음
서식 있음: 캡션, 다음 단락과의 사이에 페이지 나누기
서식 지정함: 글꼴: (한글) 바탕, 14 pt, (한글) 한국어

RMSE

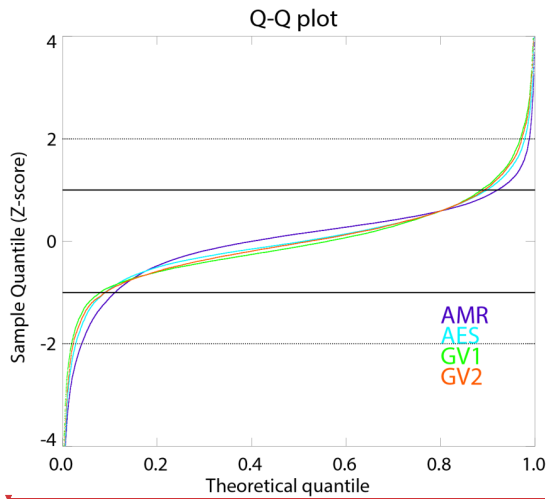


Figure 2. Q-Q plot for the difference between AERONET AOD and AMR(purple), AES(cyan), GV1(green), and GV2(orange) AOD. The black solid line and dotted line represent $1\text{-}\sigma$ and $2\text{-}\sigma$, respectively.

삭제함: 4

Table 2. RMSE values by time, AOD, and NDVI during KORUS-AQ, as used in this study RMSE. 4

삭제함: Figure 1. Comparison between observed AOD error distributions for AMR (cyan), AES (green), GV1 (yellow), and GV2 (blue). 4

서식 있음: 캡션, 다음 단락과의 사이에 페이지 나누기

삭제함: 2

서식 지정함: 글꼴: (영어) + 본문(Times New Roman), 굵게 없음

서식 지정함: 글꼴: (영어) + 본문(Times New Roman), 굵게 없음

서식 지정함: 글꼴: (영어) + 본문(Times New Roman), (한글) 바탕, (한글) 한국어

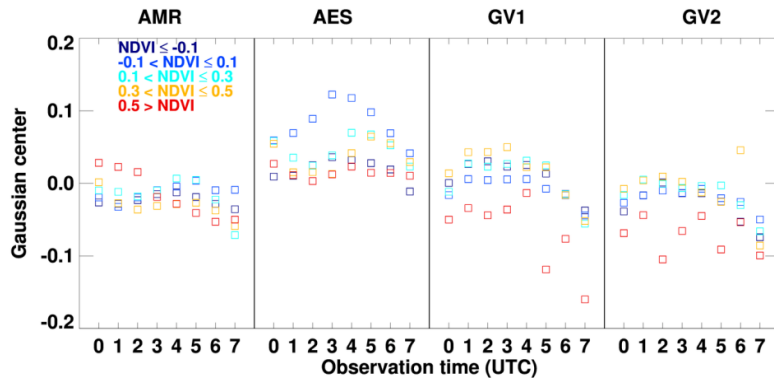



Figure 3. Systematic bias-correction values for NDVI groups and temporal bins for each satellite product from Gaussian fitting analysis used in MLE fusion.

- 서식 지정함: 글꼴: 10 pt, 굵게 없음
- 서식 있음: 캡션, 다음 단락과의 사이에 페이지 나누기
- 삭제함: 3
- 서식 지정함: 글꼴: (한글) 바탕, 14 pt, (한글) 한국어
- 서식 있음: 다음 단락과의 사이에 페이지 나누지 않음

|  (a) (b) (c) (d)

(e) (f) (g) (h)

(i) (j) (k)

| 

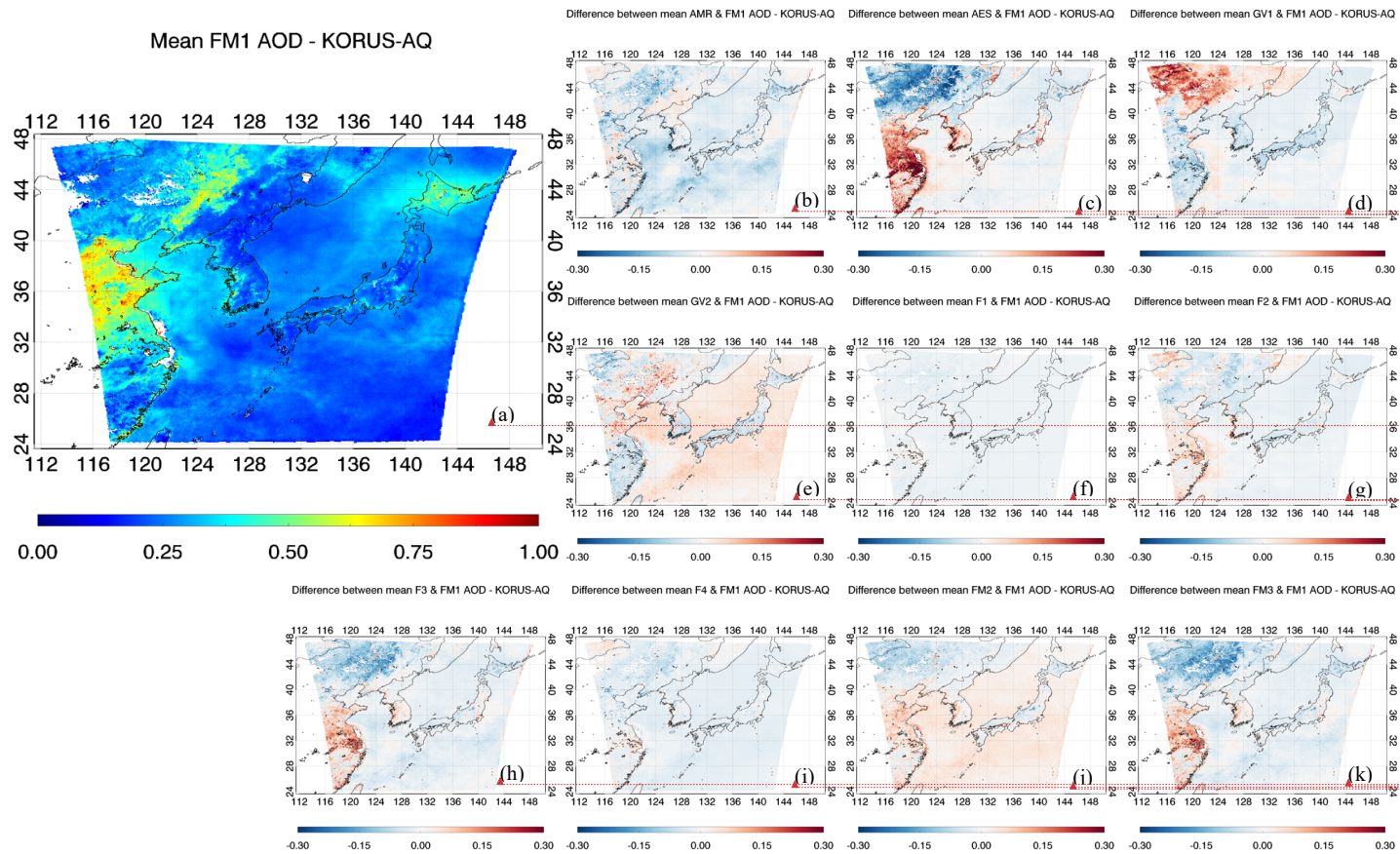


Figure 4. The average AOD of (a) FM1 (AMR, AES, GV1, and GV2) during the KORUS AQ. The difference of mean (b) AMR, (c) AES, (d) GV1, (e) GV2, (f) F1, (g) F2, (h) F3, (i) F4, (j) FM2, and (k) FM3 AODs with respect to mean representative (FM1) AOD. Figures generated with Interactive Data Language (IDL) version 8.8.0.

서식 지정함: 글꼴: (영어)+본문(Times New Roman)
 서식 지정함: 글꼴: (영어)+본문(Times New Roman)
 서식 지정함: 글꼴: (영어)+본문(Times New Roman)

서식 지정함: 글꼴: (영어)+본문(Times New Roman)

서식 지정함: 글꼴: (영어)+본문(Times New Roman)
 서식 지정함: 글꼴: (영어)+본문(Times New Roman)
 서식 지정함: 글꼴: (영어)+본문(Times New Roman)

서식 지정함: 글꼴: (영어)+본문(Times New Roman)
 서식 지정함: 글꼴: (영어)+본문(Times New Roman)
 서식 지정함: 글꼴: (영어)+본문(Times New Roman)
 서식 지정함: 글꼴: (영어)+본문(Times New Roman)
 서식 지정함: 글꼴: 10 pt, 굵게 없음
 서식 있음: 캡션
 삭제함: 4
 서식 지정함: 글꼴: 14 pt, (한글) 한국어

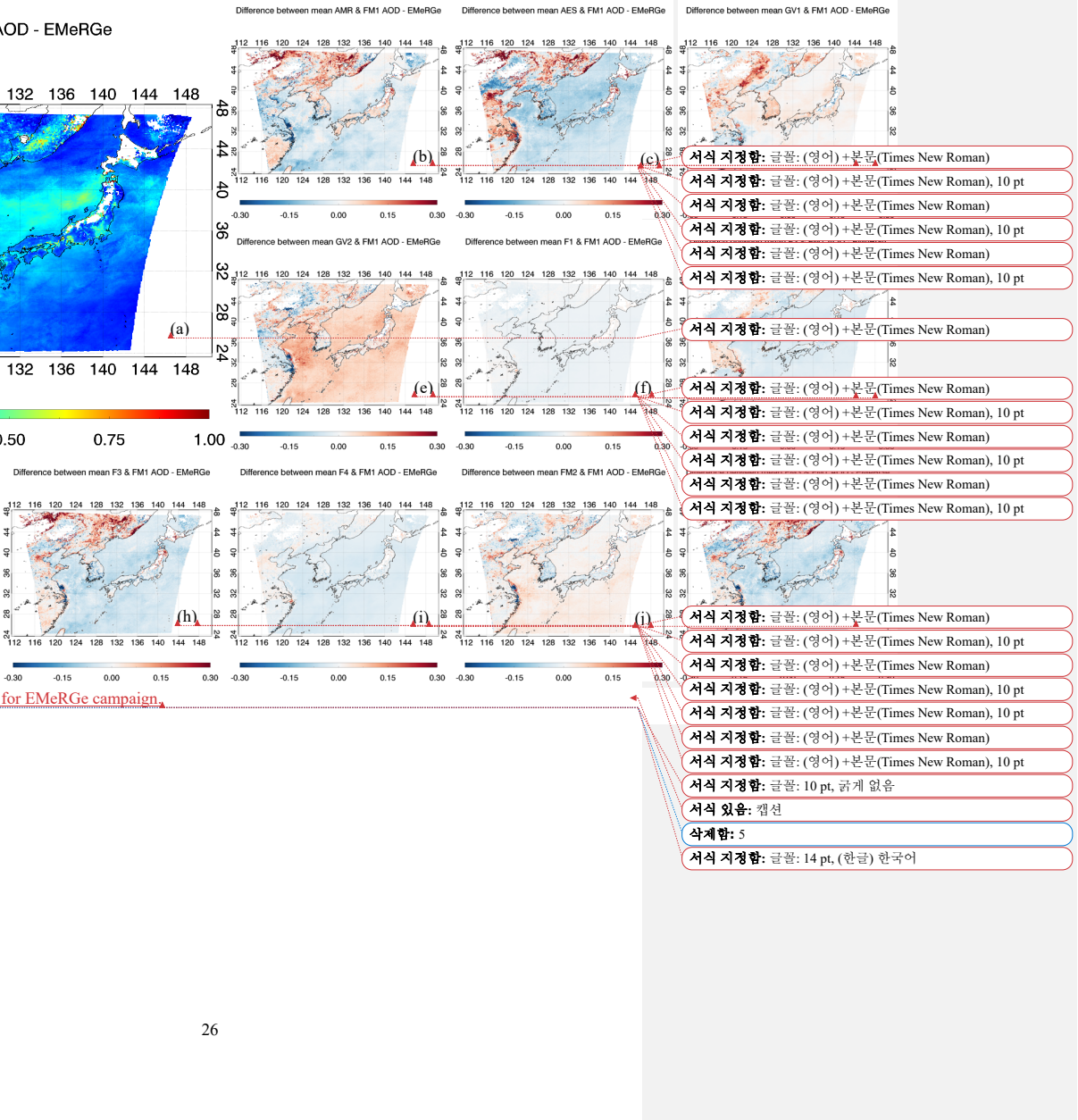
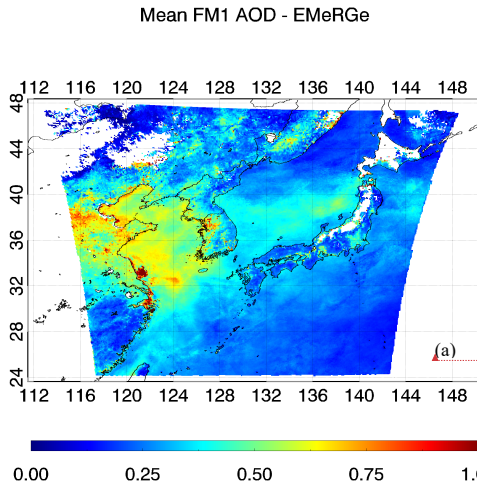


Figure 5. Same as Figure 4, but for EMeRGe campaign.

- 서식 지정함: 글꼴: (영어) + 본문(Times New Roman)
- 서식 지정함: 글꼴: (영어) + 본문(Times New Roman), 10 pt
- 서식 지정함: 글꼴: (영어) + 본문(Times New Roman)
- 서식 지정함: 글꼴: (영어) + 본문(Times New Roman), 10 pt
- 서식 지정함: 글꼴: (영어) + 본문(Times New Roman)
- 서식 지정함: 글꼴: (영어) + 본문(Times New Roman), 10 pt
- 서식 지정함: 글꼴: (영어) + 본문(Times New Roman)
- 서식 지정함: 글꼴: (영어) + 본문(Times New Roman), 10 pt
- 서식 지정함: 글꼴: (영어) + 본문(Times New Roman)
- 서식 지정함: 글꼴: (영어) + 본문(Times New Roman), 10 pt
- 서식 지정함: 글꼴: (영어) + 본문(Times New Roman)
- 서식 지정함: 글꼴: (영어) + 본문(Times New Roman), 10 pt
- 서식 지정함: 글꼴: (영어) + 본문(Times New Roman)
- 서식 지정함: 글꼴: (영어) + 본문(Times New Roman), 10 pt
- 서식 지정함: 글꼴: (영어) + 본문(Times New Roman)
- 서식 지정함: 글꼴: 10 pt, 굵게 없음
- 서식 있음: 캡션
- 삭제함: 5
- 서식 지정함: 글꼴: 14 pt, (한글) 한국어

삭제합: <개체><개체><개체><개체><개체><개체><개체><개체>
<개체><개체><개체><개체><개체><개체>
.....구역 나누기(다음 페이지부터)

삭제합: Figure 4. Time series of the (a) respective satellite-derived, (b) ensemble mean, and (c) MLE fusion AODs at Gangneung_WNU site during KORUS- AQ period.....

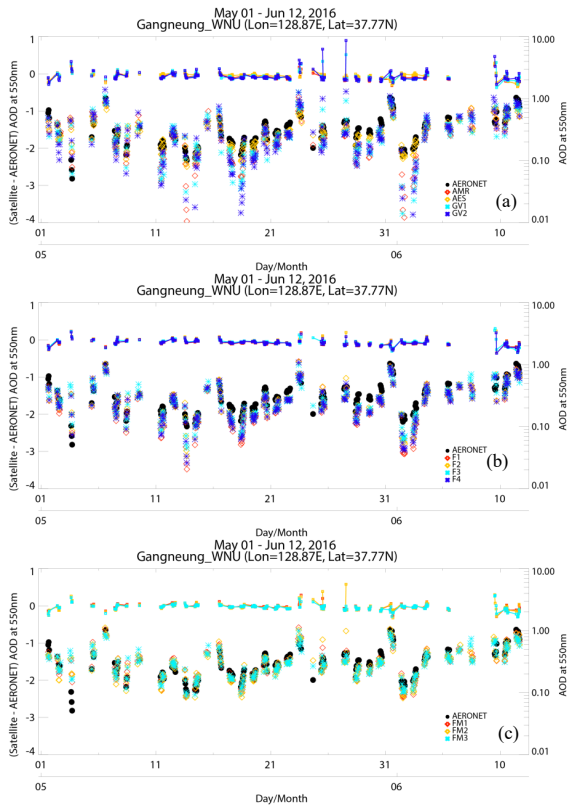


Figure 6. Time series of the AODs at Gangneung WNU site during the KORUS-AQ campaign from (a) respective satellite, (b) ensemble-mean, and (c) MLE fusion (to the right y-axis). Solid line represents difference of individual satellite retrieval from AERONET AOD at 550nm (to the left y-axis).

- 서식 지정함: 글꼴: 10 pt, 굵게 없음
- 삭제함: 6
- 서식 있음: 캡션
- 삭제함: AODs
- 삭제함: and
- 삭제함: D
- 삭제함: with
- 삭제함: , at Gangneung WNU site during the KORUS-AQ campaign
- 서식 지정함: 글꼴: 11 pt, (한글) 한국어

I
10

(a)

(e)

(i)

(b)

(f)

(j)

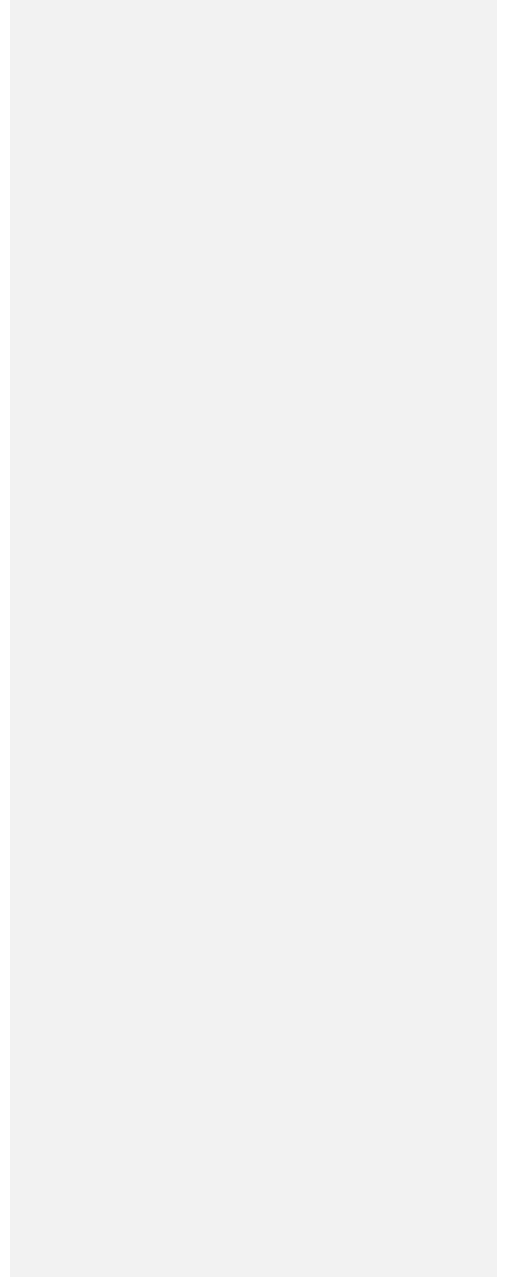
(c)

(g)

(k)

(d)

(h)



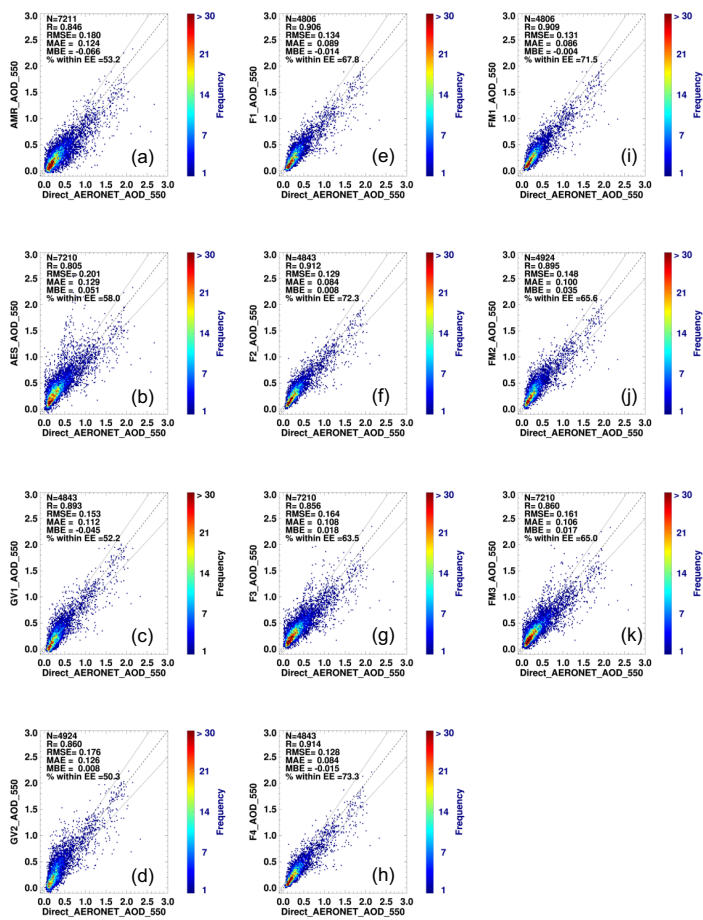


Figure 7. Comparison of four respective satellite products (a) AMR, (b) AES, (c) GV1, (d) GV2, four ensemble mean products (e) F1, (f) F2, (g) F3, (h) F4, and three MLE products (i) FM1, (j) FM2, (k) FM3 AOD with AERONETAOD during KORUS-AQ campaign.

- 서식 지정함: 글꼴: 10 pt, 굵게 없음
- 서식 있음: 캡션
- 삭제함: 7
- 서식 지정함: 글꼴: 11 pt, (한글) 한국어

삭제함: Figure 6. Spatial distribution of %EE for (a) AMR, (b) AES, (c) GV1, (d) GV2, (e) F1, (f) F2, (g) F3, (h) F4, (i) FM1, (j) FM2, and (k) FM3AOD during KORUS-AQ campaign.

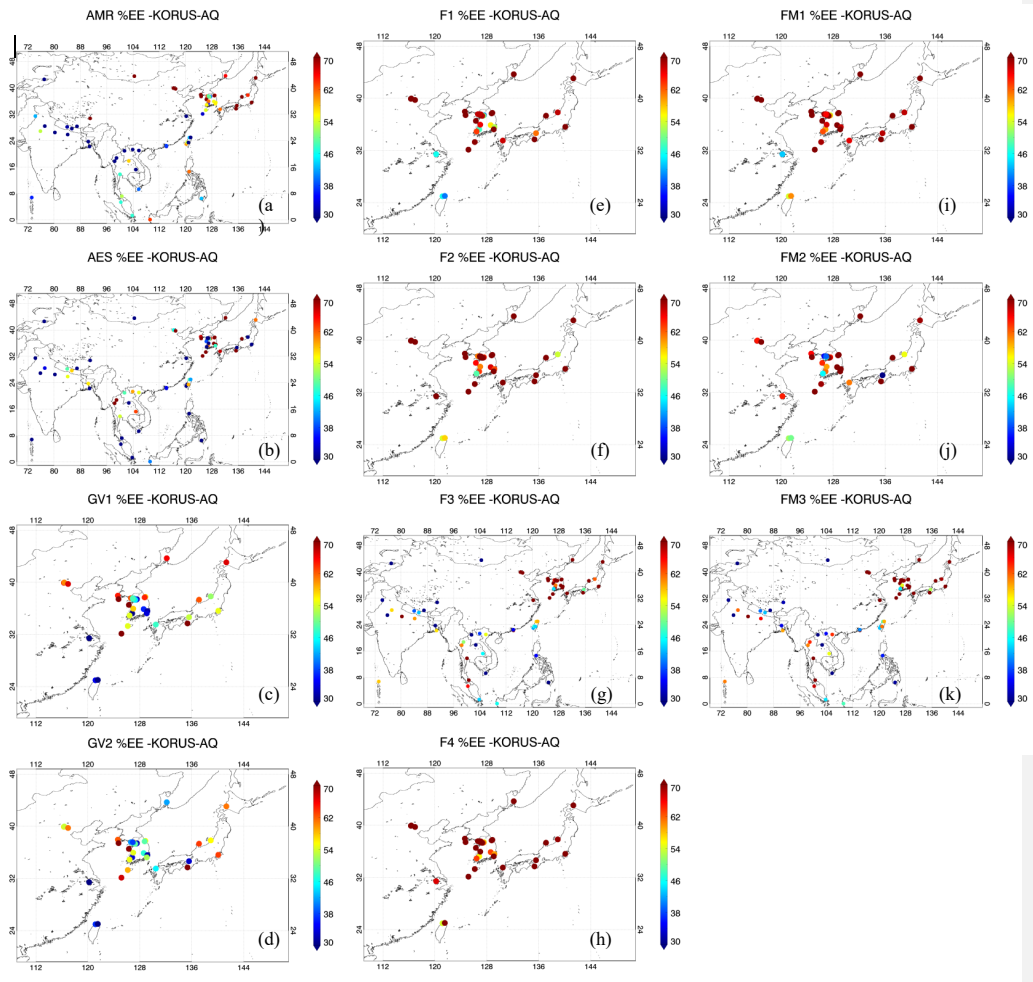


Figure 8. Spatial distribution of %EE for (a) AMR, (b) AES, (c) GV1, (d) GV2, (e) F1, (f) F2, (g) F3, (h) F4, (i) FM1, (j) FM2, and (k) FM3AOD during the KORUS-AQ campaign. Figures generated with Interactive Data Language (IDL) version 8.8.0.

서식 지정함: 글꼴: 10 pt, 굵게 없음
 서식 있음: 캡션
 삭제함: 8
 서식 지정함: 글꼴: (한글) 바탕, 11 pt, (한글) 한국어

삭제함: Figure 7. Same as Figure 5, but for EMerGe campaign

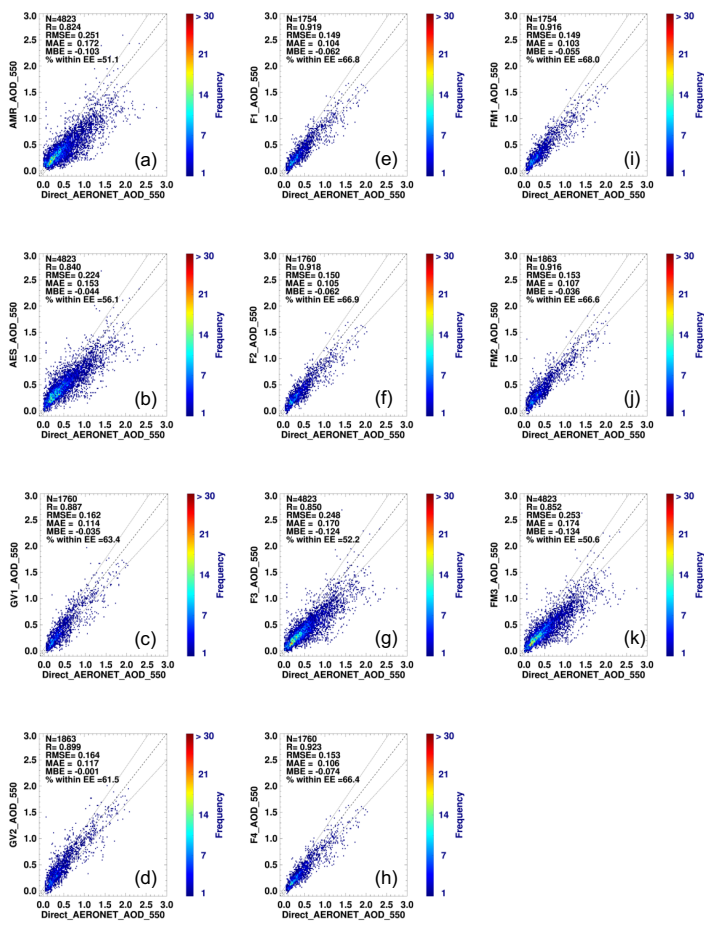
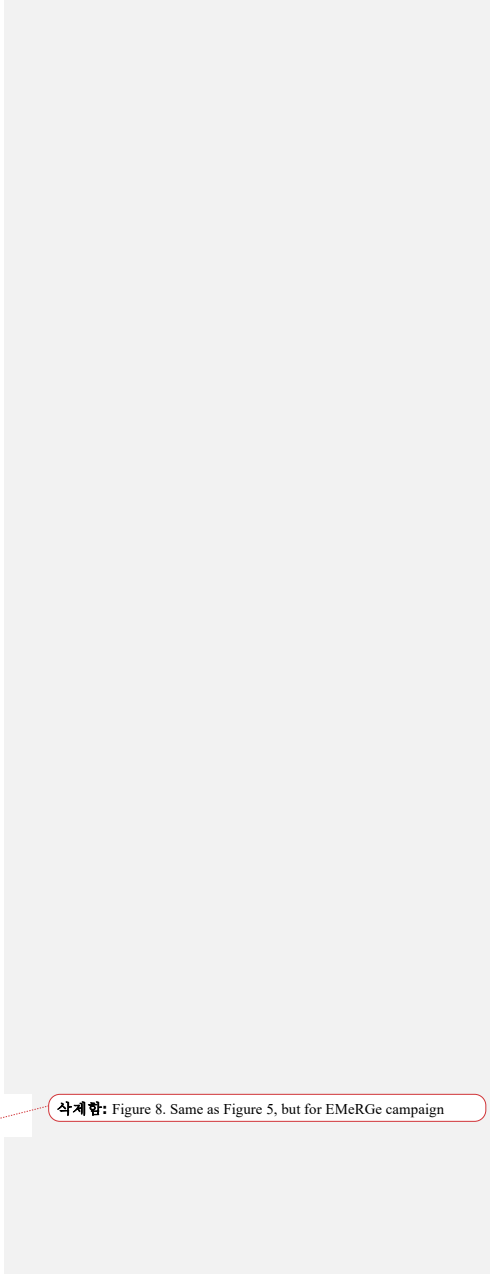


Figure 9. Same as Figure 7, but for EMERGE campaign.

- 서식 지정함: 글꼴: 10 pt, 굵게 없음
- 서식 있음: 캡션
- 삭제함: 9
- 서식 지정함: 글꼴: 11 pt, (한글) 한국어



삭제함: Figure 8. Same as Figure 5, but for EMerGe campaign

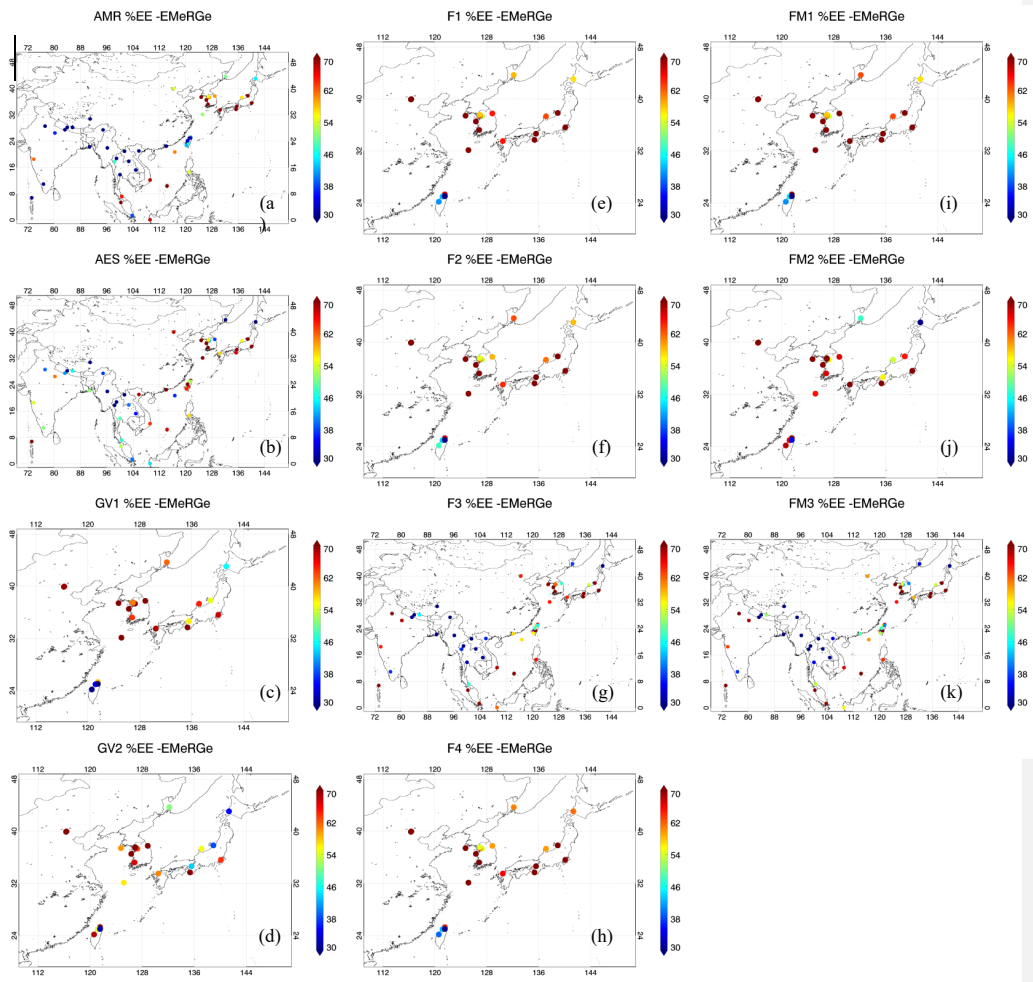


Figure 10. Same as Figure 8, but for the EMeRGe campaign.

- 서식 지정함: 글꼴: 10 pt, 굵게 없음
- 서식 있음: 캡션
- 삭제함: 10
- 서식 지정함: 글꼴: (한글) 바탕, 14 pt, (한글) 한국어

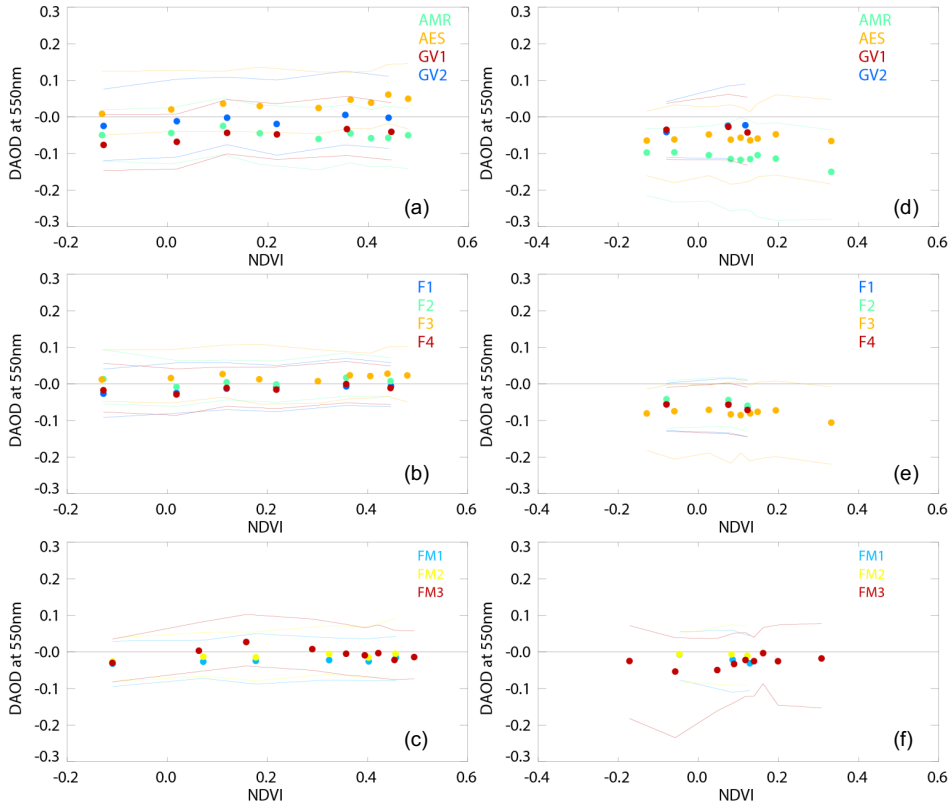


Figure 11. Difference between (a, d) respective, (b, e) ensemble-mean, or (c, f) MLE and AERONET AOD in terms of NDVI during the KORUS-AQ (left column) and the EMeRGe (right column) campaigns. Each points and solid lines represent the median and 1- σ (16th and 84th percentile) of 800 (for the KORUS-AQ) and 600 (for the EMeRGe) collocated data points in terms of NDVI values.

- 서식 지정함: 글꼴: 10 pt, 굵게 없음
- 삭제함: 11
- 서식 지정함: 글꼴: 10 pt, 굵게 없음
- 서식 지정함: 글꼴: (영어)+제목(Times New Roman)
- 서식 지정함: 글꼴: (영어)+제목(Times New Roman), 위 첨자
- 서식 지정함: 글꼴: (영어)+제목(Times New Roman)
- 서식 지정함: 글꼴: (영어)+제목(Times New Roman), 위 첨자
- 서식 지정함: 글꼴: (영어)+제목(Times New Roman)
- 서식 지정함: 글꼴: (한글) 바탕, (한글) 한국어
- 서식 지정함: 글꼴: 11 pt, (한글) 한국어
- 서식 있음: 캡션

삭제합: Figure 9. Difference between (a, d) respective, (b, e) ensemble-mean, or (c, f) MLE and AERONET/SONET AOD in terms of NDVI during the KORUS-AQ (left column) and EMerGe (right column) campaigns...

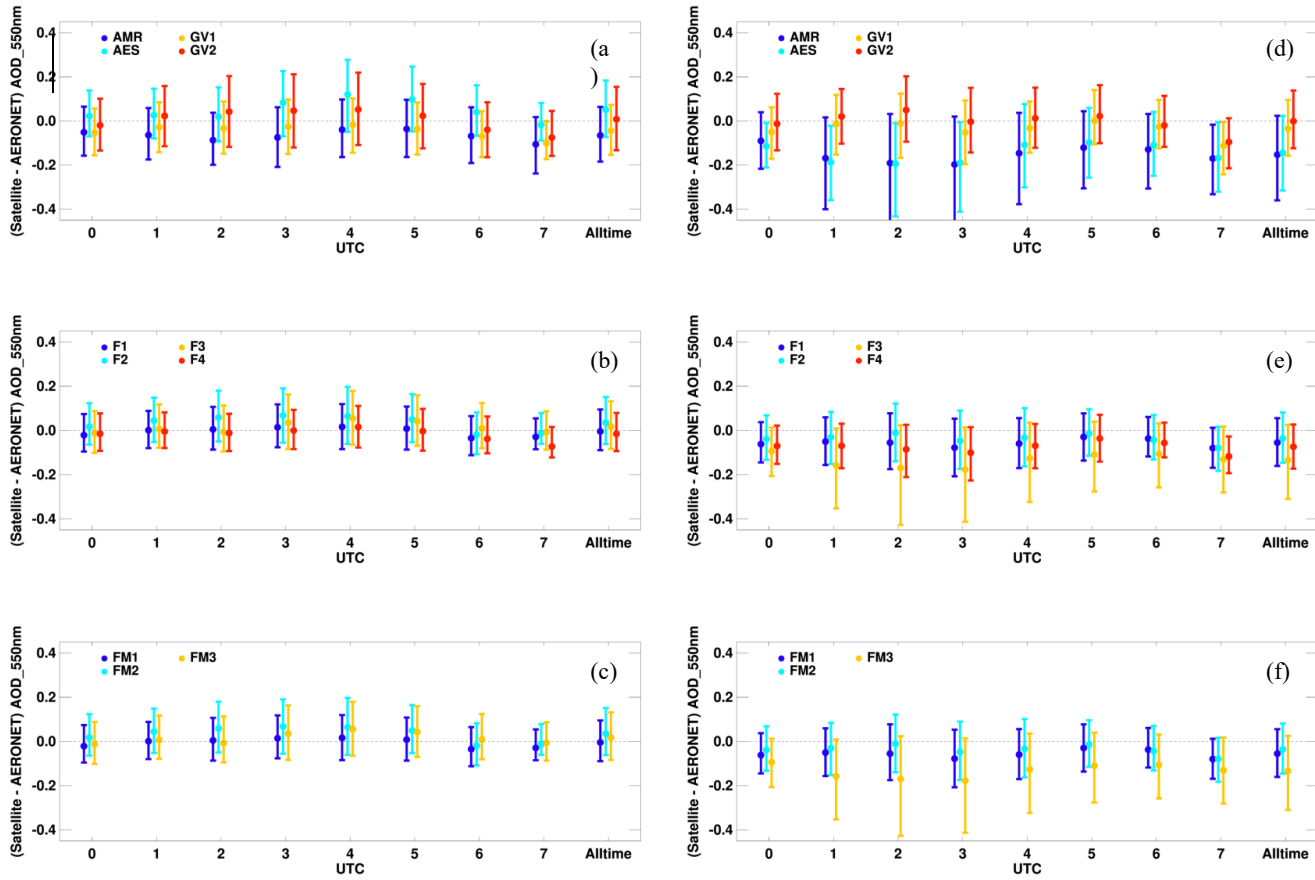


Figure 12, Same as Figure 11, but for the observation time,

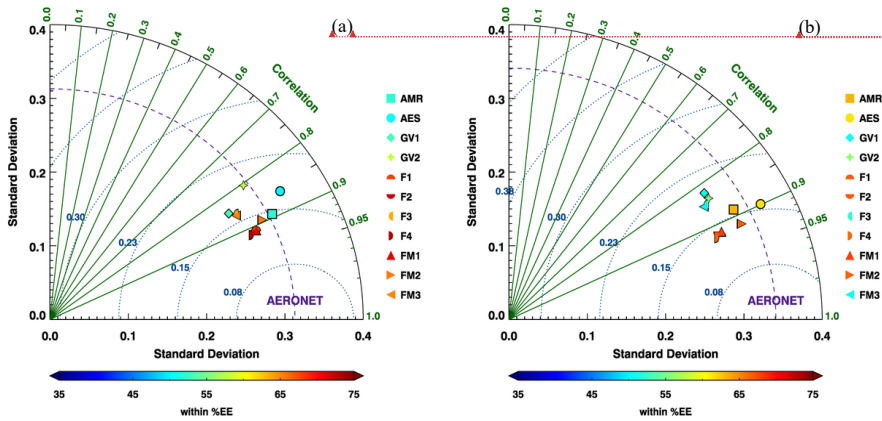
- 서식 지정함: 글꼴: 10 pt, 굵게 없음
- 서식 있음: 캡션
- 삭제함: 12
- 서식 지정함: 글꼴: (한글) 바탕, 14 pt, (한글) 한국어

35

삭제함: <개념

삭제함: Figure 10. Same as Figure 9, but for observation time.

40



서식 지정함: 글꼴: 10 pt
 서식 지정함: 글꼴: 7 pt
 서식 지정함: 글꼴: 10 pt

Figure 13. Taylor diagrams comparing the respective, ensemble-mean, and MLE AODs and values obtained from AERONET during the (a) KORUS-AQ and (b) EMERGe periods. Square, circle, diamond, star, top half circle, lower half circle, left half circle, right half circle, triangle, right-pointing triangle, and left-pointing triangle represents AMR, AES, GV1, GV2, F1, F2, F3, F4, FM1, FM2, and FM3, respectively.

서식 지정함: 글꼴: 10 pt, 굵게 없음
 서식 있음: 캡션
 삭제함: 13
 서식 지정함: 글꼴: 11 pt, (한글) 한국어

Table 2. Accuracy evaluation of GOCl area of AMR, AES, F3, and FM3 AODs.

/all / collocation with GOCl domain)	KORUS-	KORUS-	KORUS-	KORUS-	EMeRGe	EMeRGe	EMeRGe	EMeRGe
	AQ AMR	AQ AES	AQ F3	AQ FM3	AMR	AES	F3	FM3
N	7211 /-5069	7210 /-5069	7210 /-5069	7210 /-5069	4823 /-1884	4823 /-1884	4823 /-1884	4823 /-1884
R	0.846 /-0.908	0.805 /-0.905	0.856 /-0.919	0.860 /-0.922	0.824 /-0.910	0.840 /-0.892	0.850 /-0.912	0.253 /-0.911
RMSE	0.180 /-0.150	0.201 /-0.145	0.164 /-0.133	0.161 /-0.131	0.251 /-0.162	0.224 /-0.176	0.248 /-0.175	0.253 /-0.184
MBE	-0.066 /-0.054	0.051 /-0.029	0.018 /-0.012	0.017 /-0.01	-0.103 /-0.028	-0.044 /-0.011	-0.124 /-0.069	-0.134 /-0.086
%EE	53.2 /-60.6	58.0 /-63.5	63.5 /-72.1	65.0 /-72.9	51.1 /-69.4	56.1 /-65.2	52.2 /-63.2	50.6 /-60.0

- 서식 지정함: 글꼴: 10 pt, 굵게 없음
- 삭제함: 2
- 서식 지정함: 글꼴: (한글) 바탕, 10 pt, (한글) 한국어
- 서식 있음: 캡션, 다음 단락과의 사이에 페이지 나누지 않음
- 서식 지정함: 글꼴: (영어)+본문(Times New Roman)
- 서식 있는 표
- 서식 지정함: 글꼴: (영어)+본문(Times New Roman)
- 서식 지정함: 글꼴: (영어)+본문(Times New Roman)
- 서식 지정함: 글꼴: (영어)+본문(Times New Roman)
- 서식 지정함: 글꼴: (영어)+본문(Times New Roman)
- 서식 지정함: 글꼴: (영어)+본문(Times New Roman)
- 서식 지정함: 글꼴: (영어)+본문(Times New Roman)
- 서식 지정함: 글꼴: (영어)+본문(Times New Roman)
- 서식 지정함: 글꼴: (영어)+본문(Times New Roman)
- 서식 지정함: 글꼴: (영어)+본문(Times New Roman)
- 서식 지정함: 글꼴: (영어)+본문(Times New Roman)

삭제합: <개략

서식 지정합: 글꼴: (한글) 바탕

삭제합: Figure 11. Taylor diagrams comparing the respective, ensemble-mean, and MLE AODs and values obtained from AERONET during the (a) KORUS-AQ and (b) EMERGe periods.

페이지 9: [1] 삭제함 JK 2020. 12. 12. AM 11:48:00

페이지 9: [1] 삭제함 JK 2020. 12. 12. AM 11:48:00

페이지 9: [1] 삭제함 JK 2020. 12. 12. AM 11:48:00

페이지 9: [1] 삭제함 JK 2020. 12. 12. AM 11:48:00

페이지 9: [1] 삭제함 JK 2020. 12. 12. AM 11:48:00

페이지 9: [1] 삭제함 JK 2020. 12. 12. AM 11:48:00

페이지 9: [1] 삭제함 JK 2020. 12. 12. AM 11:48:00

페이지 9: [1] 삭제함 JK 2020. 12. 12. AM 11:48:00

페이지 9: [1] 삭제함 JK 2020. 12. 12. AM 11:48:00

페이지 9: [1] 삭제함 JK 2020. 12. 12. AM 11:48:00

페이지 9: [1] 삭제함 JK 2020. 12. 12. AM 11:48:00

페이지 9: [1] 삭제함 JK 2020. 12. 12. AM 11:48:00

페이지 9: [1] 삭제함 JK 2020. 12. 12. AM 11:48:00

페이지 9: [1] 삭제함 JK 2020. 12. 12. AM 11:48:00

페이지 9: [1] 삭제함 JK 2020. 12. 12. AM 11:48:00

페이지 9: [1] 삭제함 JK 2020. 12. 12. AM 11:48:00

페이지 9: [2] 삭제함 JK 2020. 12. 12. AM 11:54:00

페이지 9: [2] 삭제함 JK 2020. 12. 12. AM 11:54:00

페이지 9: [2] 삭제함 JK 2020. 12. 12. AM 11:54:00

페이지 9: [2] 삭제함 JK 2020. 12. 12. AM 11:54:00

페이지 9: [2] 삭제함 JK 2020. 12. 12. AM 11:54:00

페이지 9: [2] 삭제함 JK 2020. 12. 12. AM 11:54:00

페이지 9: [2] 삭제함 JK 2020. 12. 12. AM 11:54:00

페이지 9: [2] 삭제함 JK 2020. 12. 12. AM 11:54:00

페이지 9: [2] 삭제함 JK 2020. 12. 12. AM 11:54:00

페이지 9: [2] 삭제함 JK 2020. 12. 12. AM 11:54:00

페이지 9: [2] 삭제함 JK 2020. 12. 12. AM 11:54:00

페이지 9: [2] 삭제함 JK 2020. 12. 12. AM 11:54:00

페이지 9: [2] 삭제함 JK 2020. 12. 12. AM 11:54:00

페이지 9: [2] 삭제함 JK 2020. 12. 12. AM 11:54:00

페이지 9: [2] 삭제함 JK 2020. 12. 12. AM 11:54:00

페이지 9: [3] 삭제함 JK 2020. 12. 12. PM 3:23:00

페이지 9: [3] 삭제함 JK 2020. 12. 12. PM 3:23:00

페이지 9: [3] 삭제함 JK 2020. 12. 12. PM 3:23:00

페이지 9: [3] 삭제함	JK	2020. 12. 12. PM 3:23:00
▼		←
페이지 9: [3] 삭제함	JK	2020. 12. 12. PM 3:23:00
▼		←
페이지 9: [3] 삭제함	JK	2020. 12. 12. PM 3:23:00
▼		←
페이지 9: [3] 삭제함	JK	2020. 12. 12. PM 3:23:00
▼		←
페이지 9: [3] 삭제함	JK	2020. 12. 12. PM 3:23:00
▼		←
페이지 9: [3] 삭제함	JK	2020. 12. 12. PM 3:23:00
▼		←
페이지 9: [3] 삭제함	JK	2020. 12. 12. PM 3:23:00
▼		←
페이지 9: [3] 삭제함	JK	2020. 12. 12. PM 3:23:00
▼		←
페이지 9: [4] 삭제함	JK	2020. 12. 12. PM 3:29:00
▼		←
페이지 9: [4] 삭제함	JK	2020. 12. 12. PM 3:29:00
▼		←
페이지 9: [4] 삭제함	JK	2020. 12. 12. PM 3:29:00
▼		←
페이지 9: [4] 삭제함	JK	2020. 12. 12. PM 3:29:00
▼		←
페이지 9: [5] 삭제함	JK	2020. 12. 12. PM 3:31:00
▼		←
페이지 9: [5] 삭제함	JK	2020. 12. 12. PM 3:31:00
▼		←
페이지 9: [6] 삭제함	JK	2020. 12. 12. PM 3:30:00
▼		←
페이지 9: [6] 삭제함	JK	2020. 12. 12. PM 3:30:00
▼		←
페이지 9: [6] 삭제함	JK	2020. 12. 12. PM 3:30:00
▼		←

페이지 9: [6] 삭제함 JK 2020. 12. 12. PM 3:30:00

페이지 9: [6] 삭제함 JK 2020. 12. 12. PM 3:30:00

페이지 9: [6] 삭제함 JK 2020. 12. 12. PM 3:30:00

페이지 9: [6] 삭제함 JK 2020. 12. 12. PM 3:30:00

페이지 9: [6] 삭제함 JK 2020. 12. 12. PM 3:30:00

페이지 9: [6] 삭제함 JK 2020. 12. 12. PM 3:30:00

페이지 9: [6] 삭제함 JK 2020. 12. 12. PM 3:30:00

페이지 9: [6] 삭제함 JK 2020. 12. 12. PM 3:30:00

페이지 13: [7] 삭제함 JK 2020. 12. 12. PM 4:27:00

페이지 13: [7] 삭제함 JK 2020. 12. 12. PM 4:27:00

페이지 13: [7] 삭제함 JK 2020. 12. 12. PM 4:27:00

페이지 13: [7] 삭제함 JK 2020. 12. 12. PM 4:27:00

페이지 13: [7] 삭제함 JK 2020. 12. 12. PM 4:27:00

페이지 13: [7] 삭제함 JK 2020. 12. 12. PM 4:27:00

페이지 13: [7] 삭제함 JK 2020. 12. 12. PM 4:27:00

페이지 13: [7] 삭제함 JK 2020. 12. 12. PM 4:27:00

페이지 13: [7] 삭제함 JK 2020. 12. 12. PM 4:27:00

페이지 13: [7] 삭제함 JK 2020. 12. 12. PM 4:27:00

▼ ▲ 페이지 13: [8] 삭제함 lim 2020. 12. 7. PM 6:36:00

▼ ▲ 페이지 13: [8] 삭제함 lim 2020. 12. 7. PM 6:36:00

▼ ▲ 페이지 13: [8] 삭제함 lim 2020. 12. 7. PM 6:36:00

▼ ▲ 페이지 13: [8] 삭제함 lim 2020. 12. 7. PM 6:36:00

▼ ▲ 페이지 13: [8] 삭제함 lim 2020. 12. 7. PM 6:36:00

▼ ▲ 페이지 13: [8] 삭제함 lim 2020. 12. 7. PM 6:36:00

▼ ▲ 페이지 13: [8] 삭제함 lim 2020. 12. 7. PM 6:36:00

▼ ▲ 페이지 13: [8] 삭제함 lim 2020. 12. 7. PM 6:36:00

▼ ▲ 페이지 13: [8] 삭제함 lim 2020. 12. 7. PM 6:36:00

▼ ▲ 페이지 13: [8] 삭제함 lim 2020. 12. 7. PM 6:36:00

▼ ▲ 페이지 13: [8] 삭제함 lim 2020. 12. 7. PM 6:36:00

▼ ▲ 페이지 13: [8] 삭제함 lim 2020. 12. 7. PM 6:36:00

▼ ▲ 페이지 13: [8] 삭제함 lim 2020. 12. 7. PM 6:36:00

▼ ▲ 페이지 13: [8] 삭제함 lim 2020. 12. 7. PM 6:36:00

▼ ▲ 페이지 13: [8] 삭제함 lim 2020. 12. 7. PM 6:36:00

▼ ▲ 페이지 13: [8] 삭제함 lim 2020. 12. 7. PM 6:36:00

▼ ▲

페이지 13: [8] 삭제함	lim	2020. 12. 7. PM 6:36:00
▼		←
▲ 페이지 13: [8] 삭제함	lim	2020. 12. 7. PM 6:36:00
▼		←
▲ 페이지 13: [8] 삭제함	lim	2020. 12. 7. PM 6:36:00
▼		←
▲ 페이지 13: [8] 삭제함	lim	2020. 12. 7. PM 6:36:00
▼		←
▲ 페이지 13: [8] 삭제함	lim	2020. 12. 7. PM 6:36:00
▼		←
▲ 페이지 13: [8] 삭제함	lim	2020. 12. 7. PM 6:36:00
▼		←
▲ 페이지 13: [8] 삭제함	lim	2020. 12. 7. PM 6:36:00
▼		←
▲ 페이지 13: [8] 삭제함	lim	2020. 12. 7. PM 6:36:00
▼		←
▲ 페이지 13: [8] 삭제함	lim	2020. 12. 7. PM 6:36:00
▼		←
▲ 페이지 13: [8] 삭제함	lim	2020. 12. 7. PM 6:36:00
▼		←
▲ 페이지 13: [8] 삭제함	lim	2020. 12. 7. PM 6:36:00
▼		←
▲ 페이지 13: [8] 삭제함	lim	2020. 12. 7. PM 6:36:00
▼		←
▲ 페이지 20: [9] 삭제함	lim	2020. 12. 3. PM 1:56:00
▼		←
▲ 페이지 24: [10] 삭제함	lim	2020. 12. 3. PM 6:11:00
▼		←
▲		←